Thesis for the degree of doctor of philosophy

Charge storage mechanisms and interactions of hybrid supercapacitor electrode materials with next-generation electrolytes

Simon Lindberg

CHALMERS

Department of Physics
Chalmers University of Technology
Göteborg, Sweden 2020

Charge storage mechanisms and interactions of hybrid supercapacitor electrode materials with next-generation electrolytes

Simon Lindberg

ISBN 978-91-7905-291-1

Doktorsavhandlingar vid Chalmers tekniska högskola,
Ny serie nr 4758.
ISSN 0346-718X.

Department of Physics
Chalmers University of Technology
SE-41296 Göteborg
Sweden

Chalmers Reproservice
Göteborg, Sweden 2020

Charge storage mechanisms and interactions of hybrid supercapacitor electrode materials with next-generation electrolytes

Simon Lindberg
Department of Physics
Chalmers University of Technology
SE-41296 Göteborg, Sweden

Abstract

The storage of electrical energy is of outmost importance in today's society for a wide range of applications. Batteries, that are most common for electrical energy storage today, struggle with low power density and limited cycle lifetime. As an alternative to batteries, supercapacitors have a high-power density and almost unlimited cycle lifetime. However, the lower energy content of supercapacitors limits their use in different applications.

Two properties determine the energy content of supercapacitors: the capacity of the electrodes and operating voltage of the device. Metal oxides have a high capacity compared to standard carbon electrodes. In this thesis MnO_2, VO_2 and TiO_2 are investigated together with novel electrolytes. Previously these materials have been mostly studied in standard aqueous electrolytes. Ionic liquids (ILs) is a class of novel solvents which can be more stable than aqueous electrolytes and mitigate problems associated with organic electrolytes. Another electrolyte concept receiving increasing interest is highly concentrated electrolytes (HCEs) in which the high salt concentration makes the electrolyte electrochemically stable. The electrode-electrolyte interaction is governed by the choice of electrolyte but also the morphology of the electrode

In this work I present findings that could facilitate the development of next-generation hybrid supercapacitors with improved energy density as a result of high-capacity electrodes and novel electrolytes. By choosing appropriate electrolytes a higher capacity of the electrode could be obtained together with an increased voltage window, increasing the energy density further. I also present findings regarding the morphology and structure of the electrode. Examples of key results include the role of protic ionic liquids in the charge storage in electrodes with transition metal oxides, the possibility to increase the voltage window by using a highly-concentrated electrolyte exploiting additional faradaic processes and the mitigation of the capacity fade in TiO_2 by the use of an ionic liquid electrolyte.

Keywords: Supercapacitors, Ionic liquids, Hybrid supercapacitors, MnO_2, Charge storage mechanism, TiO_2, VO_2, Highly-concentrated electrolyte.

List of Publications

This thesis is based on the work contained in the following papers:

I. Comparison of ionic liquid electrolyte to aqueous electrolytes on carbon nanofibres supercapacitor electrode derived from oxygen-functionalized graphene
K. O. Oyedotun, T. M. Masikhwa, S. Lindberg, P. Johansson, A. Matic and N. Manyala
Chemical Engineering Journal 375, 121906 (2019), https://doi.org/10.1016/j.cej.2019.121906

II. Study of the charge storage mechanism of alpha-MnO_2 in protic and aprotic ionic liquid electrolytes
S. Lindberg, S. Jeschke, P. Jankowski, M. Abdelhamid, T. Brousse, J. Le Bideau, P. Johansson and A. Matic
Journal of Power Sources 460, 228111 (2020),
https://doi.org/10.1016/j.jpowsour.2020.228111

III. Electrochemical interaction between a self-standing epsilon-MnO_2/CNF electrode and ionic liquids
S. Lindberg, M. Sadd, S. Xiong, J. Heo, J.H. Ahn, A. Matic
In manuscript

IV. Electrochemical behaviour of Nb-doped anatase TiO_2 microbeads in an ionic liquid electrolyte
S. Lindberg, C. Cavallo, G. Calcagno, A. M. Navarro-Suarez, P. Johansson, and A. Matic
Under review

V. Fast Charging Negative Electrodes based on Anatase Titanium Dioxide Beads for Highly Stable Hybrid Asymmetric Supercapacitors
G. Calcagno, A. Dang, A. Lotsari, S. Lindberg, A. E.C. Palmqvist, A. Matic and C. Cavallo,
Under review

VI. A VO_2 based hybrid super-capacitor utilizing a highly concentrated aqueous electrolyte for increased potential window and capacity
S. Lindberg, N. Maty Ndiaye, N. Manyala, P. Johansson and A. Matic
Electrochimica Acta (2020), https://doi.org/10.1016/j.electacta.2020.136225

Contribution report

Paper I.
I assisted in choosing suitable electrolytes and discussed the results with my coauthors. I contributed to writing the paper, in particular the parts concerning the ionic liquid, an assisted in finalizing the paper.

Paper II.
I designed the experiments and proposed the ionic liquids to be investigated. I did all the electrochemical measurements and analysis of the experimental and theoretical results. I discussed all results with the coauthors. I wrote the first draft of the paper, excluding the parts concerning the computational methods, and finalized the paper with the coauthors.

Paper III.
I did the preliminary electrochemical characterization of the composite electrodes in the protic ionic liquid and proposed which composition that was optimal for the study. I interpreted the Raman, XRD and XPS results. I wrote the manuscript with input from the coauthors.

Paper IV.
I did the electrochemical measurements, including the impedance spectroscopy, assisted in the design of the material, i.e. selecting the suitable doping level, and interpretation of the results. I wrote the first draft for the paper and finalized the paper with the coauthors.

Paper V.
I assisted in the 3-electrode measurements and was involved in the discussions on the results and conclusions, and discussed the manuscript together with the other authors.

Paper VI.
I assisted in the synthesis of the electrode materials, prepared the electrolytes and electrodes. I performed the electrochemical measurements and the interpretation of the results. I discussed all results with my coauthors as well as wrote the first draft for the paper and finalized the paper with the coauthors.

List of acronyms

CNF	Carbon nanofiber
MnO_2	Manganese dioxide
VO_2	Vanadium dioxide
TiO_2	Titanium dioxide
RuO_2	Ruthenium dioxide
IL	Ionic liquids
HCE	Highly-concentrated electrolytes
EDLC	Electric Double Layer Capacitor
SHE	Standard Hydrogen Electrode
TEA	Tetraethylammonium
BF_4	Tetrafluoroborate
TFSI	Bis(trifluoromethanesulfonyl)imide
KOH	Potassium hydroxide
BMIM	1-butyl-3-methylimidazolium
EMIM	1-ethyl-3-methylimidazolium
EIM	1-ethylimidazolium
SBIM	1-(4-sulfobutyl)-3-methylimidazolium
ACN	Acetonitrile
DEME	Diethyl-(methyl-2-methoxyethyl)-ammonium
PYR14	1-butyl-1-methylpyrrolidinium
Et3NH	Triethylammonium
EtOHIM	1-ethanol-3-methylimidazolium

Table of contents

1. Introduction

The storage of electrical energy is of outmost importance in today's society, in applications ranging from cell phones to large scale energy storage of intermittent electricity sources. Batteries, that are most commonly used as electrical energy storage today, struggle with low power density and limited cycle lifetime [1]. As an alternative to batteries, supercapacitors have a high-power density and almost unlimited cycle lifetime. However, supercapacitors have much lower energy density which limits their use in different applications where they otherwise would have been suitable [2]. To improve the feasibility of supercapacitors in applications such as the automotive industry, the energy density of 2 – 8 Wh/kg for current devices needs to be increased to > 15 Wh/kg with a maintained power performance [2].

Two factors that directly affect the energy density of a supercapacitor is the capacity of the electrodes and the operating voltage of the device [3]. Carbon, which is the most common electrode material today has a low capacity. Metal oxides, such as MnO_2, RuO_2 or VO_2, have higher capacities than carbon and are being studied extensively as a way to increase the capacity of electrodes in supercapacitors [4–7]. The main factor limiting the voltage window of devices is the electrochemical stability of the electrolyte. If polarized to sufficiently high or low potentials the electrolyte will decompose which eventually kills the cell. The potential limits of the electrolyte depend on the electrochemical stability, for example water, which is a very good solvent for many applications, is limited to an upper potential of 1.23 V [8] before it is split into oxygen gas and H_3O^+.

Organic electrolytes consisting of a salt dissolved in an organic solvent are most commonly used in commercial supercapacitors today, enabling voltage windows up to 2.8 V. Acetonitrile is the preferred solvent due to the higher conductivity and ability to dissolve salts, however, it has a relatively high toxicity and flammability. Electrolytes for future supercapacitor applications should have high conductivity, electrochemical stability, non-flammability and high temperature stability. Suggested next-generation electrolytes are novel organic solvent-based electrolytes, ionic liquids and highly-concentrated electrolytes [9–11]. Of these concepts, ionic liquids and highly-concentrated aqueous electrolytes have been considered promising for next-generation supercapacitors with the potential to fulfill several of the criteria above.

To increase the energy density of supercapacitors, the application of high-capacity electrodes and electrochemically stable electrolytes have previously mostly been investigated separately [8,12]. In this thesis the two approaches are combined and the aim is to develop an understanding of the charge storage mechanism in non-conventional electrolytes and how the interaction between the electrolyte and the active electrode material affects properties such as cycle lifetime and capacity. The research is focused around the interaction between faradaic electrode materials and ionic liquid electrolytes and highly concentrated electrolytes.

Three common metal oxides (MnO_2, VO_2 and TiO_2) have been explored as active materials in the electrodes with ionic liquids to investigate the charge storage mechanism. This was investigated by using MnO_2 electrodes and selectively choose similar ionic liquids but with very different hydrogen bond forming ability. Furthermore, the charge storage mechanism of MnO_2 and TiO_2 with an IL containing Li-ions was investigated. For the highly concentrated electrolyte, the question was if it could both increase the capacity of the electrode and increase the potential window. In addition, how different morphologies of metal oxide electrodes affect the charge storage mechanism and interaction with the novel electrolytes has also been addressed. Increasing the knowledge around these fundamental issues can help to tailor future hybrid electrodes to suite ionic liquids and highly concentrated electrolytes in order to exploit their full potential to increase the energy density of the next-generation supercapacitors.

2. Supercapacitors

The first description of an energy storage device resembling a supercapacitor was presented by H. I. Becker in a patent from 1954 [13]. He presented an energy storage device based on activated carbon electrodes that had a large capacitance compared to the capacitors of that time. The concept was not immediately commercialized and the term 'supercapacitor' was instead invented by NEC in 1978 as they commercialized supercapacitors for back-up memories in computers [14].

In this thesis the supercapacitor family is separated in two categories, Electric Double Layer Capacitors (EDLC) and hybrid supercapacitors (HSC). EDLCs are based on the first supercapacitors invented in 1954, with a salt containing solvent as electrolyte and the charge is stored as double layers at the surface of the electrode. HSCs are devices where a faradaic material is added to the electrode, which will enable the charge not only to be stored as double layers but also through electrochemical processes, resulting in a higher charge storage capacity. The two categories are schematically visualized in Figure 1.

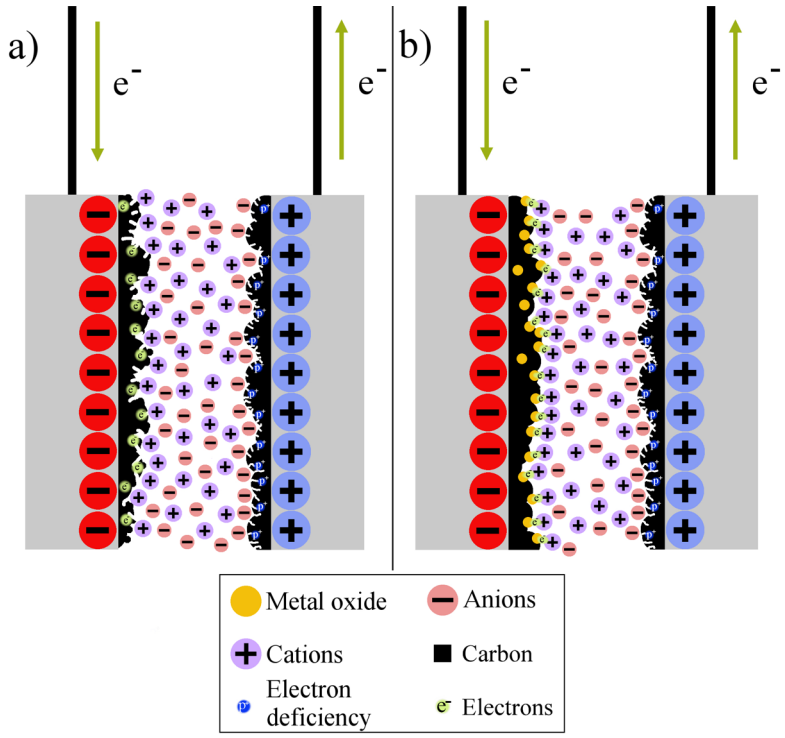

Figure 1. Schematic cell setup of a) an EDLC and b) a hybrid HSC.

EDLC devices are the most common type of supercapacitors on the market today [15]. The reason is the high-power density, more than 10 times that of Li-ion batteries and, a cycle lifetime of more than 10^6 cycles. Thanks to these unique properties supercapacitors have found their way into applications were high power is of interest rather than high energy. Examples of such applications are flash chargers [16], opening the emergency doors of the Airbus A380 'Dreamliner' [17] and as a power source for avalanche airbags used in off-pist skiing [18]. There are also examples of supercapacitor applications which are crossing into traditional Li-ion battery territory, e.g. energy storage for electrical bus prototypes [19]. However, despite

these emerging applications there is a need to increase the energy density of supercapacitors to enable their use in applications demanding higher energy density and high power density [2].

A Ragone plot is often used to visualize the energy-power regions that different energy storage devices operate in [20]. In a Ragone plot the energy and power densities are plotted in the same figure, as shown in the example in Figure 2. where the typical energy/power regions of Li-ion batteries, capacitors and supercapacitors are compared to the suggested region for next-generation HSCs [3,21]. As examples of the state-of-the-art supercapacitors, data for three commercial supercapacitors have been added (according to the datasheets available on the home page of each manufacturer [22–24]). Approximate discharge times for the devices can be obtained from the diagonal lines in the Ragone-plot, which for next-generation supercapacitors should be in the range 36 s to 6 minutes. In this specific Ragone-plot the gravimetric energy and power densities are compared. However, it is equally important to evaluate the volumetric densities as well since for some applications the volume available is limited. The 102V 88F module in Figure 2 has volumetric energy and power densities of 4.3 Wh/L and 11.6 kW/L.

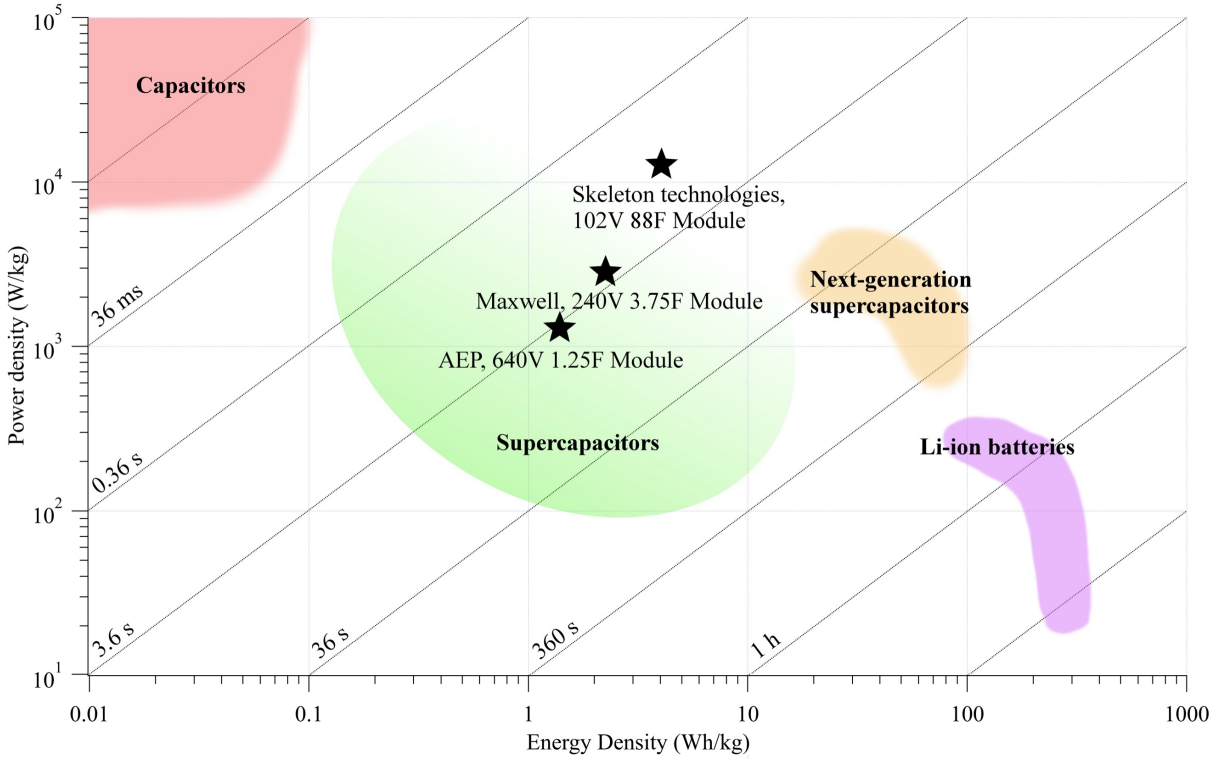

Figure 2. A Ragone plot indicating the approximate energy/power densities for a selection of state-of-the-art electrical energy storage technologies as well as the desired performance for next-generation supercapacitors and the performance of three commercial supercapacitor modules.

The aim with my thesis work has been to investigate new combinations of materials and electrolytes for HSCs to enable reaching the energy and power density region of next-generation supercapacitors marked in Figure 2. The increased energy density compared to the current supercapacitors is the biggest hurdle to overcome while keeping good power performance. These two characteristics often put contradicting demands on material properties and electrode design.

The energy content of a device depends on the charge stored in the electrodes and in which potential window the device operates. The charge, is defined as the number of electrons inserted or extracted from an electrode. For capacitors and EDLCs, the stored charge has historically expressed as capacitance, C, which is defined as

$$C = \frac{Q}{V} \quad (1)$$

where Q is the charge inserted in the electrode and V the potential in which the electrode is cycled. For (1) to be applicable the charge increase should be constant for a certain potential step, a capacitance of 1 F means that 1 As increases the voltage 1 V. This is characterized as linear change in the potential profile at charge and discharge, compared to the non-linear potential profile of a faradaic material, showed as an example in Figure 3.

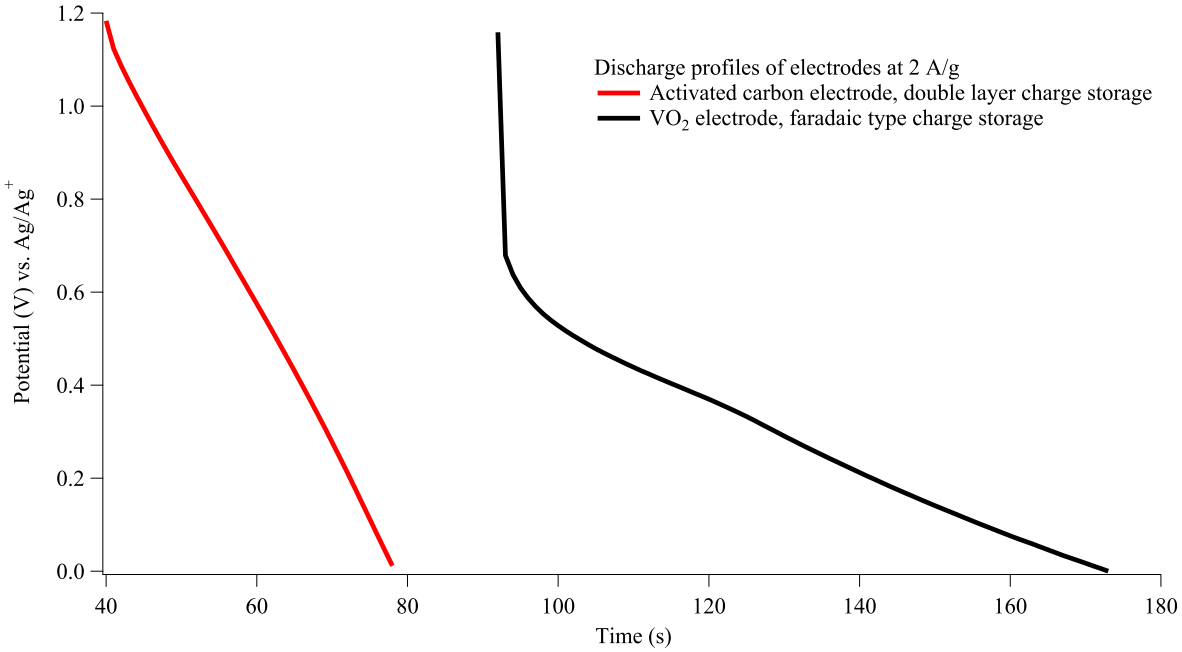

Figure 3. Comparison of the potential profiles during discharge of activated carbon with a linear double layer charge storage and VO_2 with a non-linear faradaic charge storage.

These potential profiles in Figure 3 where acquired at a current density of 2 A/g, the capacitance of the activated carbon is calculated as C_{carbon} = 67 F/g while the battery type material will have a capacity of Q_{VO2} = 46 mAh/g. The easiest way to compare these results is to convert F/g to mAh/g by multiplying the capacitance with the potential window and dividing with 3.6, from the conversion of As to mAh, resulting in a specific capacity of Q_{carbon} = 22 mAh/g. This conversion needs to be performed when comparing figures of merits of battery type and double layer materials where the charge storage commonly is stated in mAh/g and G/g respectively. Capacitance can only be used on materials with linear potential profiles, regardless if the charge storage comes from double layer formation or electrochemical reactions. Some materials like RuO_2 show potential profiles similar to that of double layer formation, but significantly larger. This effect is often referred to as pseudocapacitance [7,25].

The amount of charge stored in a device is limited by the electrode with the lowest capacity. This can be understood by viewing the electrodes as individual capacitors connected in a series. When charged, the smallest capacitor will be charged first and prevent the bigger capacitor to

be fully charged, which will result in a device with a lower specific capacitance than if the electrodes where properly balanced. The charge of a device can be described as

$$\frac{1}{Q_{device}} = \frac{1}{Q_2} + \frac{1}{Q_1} \quad (2)$$

where Q_1 and Q_2 is the capacity of the individual electrodes [26]. If the electrodes have equal capacity, then, $Q = Q_1 = Q_2$ and the capacity of the device is $Q_{device} = 0.5*Q$.

For EDLC devices, when using capacitance as the unit of measure, the energy content follows

$$E \propto CV^2 \quad (3)$$

while for non-linear potential profiles, when using capacity as the unit of measure, it follows

$$E \propto QV \quad (4)$$

where V is the width of the voltage window in which the device operates. By increasing the voltage window, it is possible to increase the energy content. This is most often achieved by using electrolytes with wider potential windows, which will be further discussed below.

The power content of a supercapacitor device, can be expressed as

$$P_{max} \propto \frac{V_{max}^2}{ESR} \quad (5)$$

where ESR is the equivalent circuit resistance, in other words the total resistance of all parts in the supercapacitor cell. Low resistance of the electrode materials is therefor critical to optimize the power content. The reactions that occur at the electrodes and the transport of ions in the electrolytes should be fast regardless of which setup is used and a larger potential window also increases the power density.

2.1 Supercapacitor components

The two most important parts regarding the energy and power content of supercapacitors is the electrolyte and electrode, that make up more than 50 % of the total cost of a device [2]. However, other components of the device also need to be taken into consideration. The separator for example, that separates the negative and the positive electrode can be modified to reduce the volume of cell and reduce the electrolyte needed which improves the energy and power densities by reducing the resistance of the electrolyte. The current collectors, on which the electrodes are deposited adds extra weight and cost, up to 58 % of the electrode cost comes from the current collector [2]. Using self-standing electrodes would save weight and cost but the conductivity needs to be exceptional not to reduce the power output.

2.2 Electrolytes

The electrolyte plays an important role in increasing the energy content of the device by determining the voltage window. This applies to both HSCs and EDLC devices. The most common electrolytes for EDLCs are salts dissolved in organic solvents, such as tetraethylammonium tetrafluoroborate in acetonitrile or propylene carbonate. These

electrolytes have the benefits of relative high conductivity, low viscosity and low cost. They can be cycled in a voltage window of 2.85 V. To further increase the electrochemical stability window of the electrolyte, there are a couple of different approaches that can be used. One way to increase the electrochemical stability of salt-in-solvent type electrolytes is to increase the salt concentration [27], or use ionic liquid electrolytes potential windows of up to 4.5 V [28]. A more in-depth discussion about electrolytes is found in the Electrolytes chapter.

2.3 Carbon electrode materials

The original concept of charge storage in activated carbon electrodes have remained and are used in the devices indicated in Figure 2. Today it is known that the charge stored in activated carbon electrodes are from the formation of double layers at the electrode surface as the potential is changed. This is the main reason for the high-power performance of supercapacitors [3].

The most important property of carbon materials for supercapacitor electrodes is the large specific surface area since the charge stored is proportional to the available surface. The pore distribution is important since it governs the access of ions to the surface of the carbon, too small pore sizes compared to the ions in the electrolyte can limit the accessibility. The conductivity is also important due to the high-power operation of supercapacitors.

By changing the process parameters in the synthesis of carbon materials, it is possible to tune the pore-size distribution and conductivity. Carbon derived from biomass can have capacities ranging from about 120 to 300 F/g [29]. The most common commercially available carbons used in EDLC are derived from coconut husks and have a capacitance of around 100 F/g, a surfaceof 2347 m^2/g and an average pore size of 1.3 nm [2]. More recently discovered carbon allotropes such as graphene and nanotubes have also been investigated as electrode materials but no dramatic improvement in capacitance has so far been obtained [2]. When summarizing the discussion above, it is challenging to imagine how to increase the capacitance of future EDLC materials the 60 % needed for future applications [2] using only carbon materials.

2.4 Faradaic electrode materials

By combining traditional supercapacitor materials such as activated carbon, with materials that interacts electrochemically with the electrolyte, it is possible to increase the energy density of a device. Metal oxides such as RuO_2 was first suggested as an electrode material by Trasatti et al in 1971 [30] and investigated in 1975 by B. E. Conway [31] as supercapacitor electrodes. This laid, in many ways, the foundation for the faradaic electrodes being researched today for supercapacitor applications.

The research and development of these faradaic electrode materials is primarily focused on the specific capacity which is determined by the number of electrons that can be extracted or inserted into the material. Current research span from affordable, yet high-performing ,conductive polymers, which can reach around 700 F/g [32], to metal oxides with varying degree of rarity, ranging from MnO_2 [33] with 462 F/g to RuO_2 [34] which can deliver 1500 F/g. However, while many metal oxides, like RuO_2, show excellent performance it is important to realize that these materials can be prohibitively expensive and will never make into commercial devices despite stellar performance [2].

In this project the faradaic materials were separated into two categories: Surface active redox materials and insertion type materials, which have different properties regarding energy density, power density and cyclability. The cyclability is very important but not visible in a Ragone-plot. Insertion-type materials uses the bulk of the material which can lead to strain on the material, and can shorten the cycle lifetime compared to the minimum of 10^6 cycles with EDLC devices. In general cycle lifetime of insertion type materials are often rated as 'good' or 'excellent' even when loosing up to 40 % of the initial capacity within the first couple of thousand cycles [35–37] . While this might be excellent for a battery, better cycle lifetime is required to substitute EDLC devices in applications. However, there are materials, e.g. $Li_4Ti_5O_{12}$, that has proven a cycle lifetime of up to 10k with negligible capacity loss [38]. A common method to mitigate the negative effects by ion-insertion is to nanosize the material, e.g. demonstrated for $LiMn_2O_4$ [39] where decreasing the particle size from 70 to 40 nm leads to a substantial improvement of the cycle lifetime. When it comes to surface active redox materials, a better cycle lifetime than insertion type materials can in principle be expected. However, similar issues as for insertion-type materials of cyclability can be found for various surface active redox materials [40,41], but a larger fraction of the results published do exhibit good cyclability over a couple of thousand cycles [42,43] or even over 10k-25k cycles [44–46].

To compare the energy and power densities of state-of-the-art insertion and surface-active redox materials a selection of literature results of full cells based on these materials are plotted in a Ragone-plot in Figure 4, note that the power and energy densities are normalized only to the electrode mass. The two layered structures, MoS_2 and the MXene ($Ti_3C_2T_x$) perform best, even compared to RuO_2 which is seen as one of the best materials for HSCs. Also, the difference in performance to the more traditional $LiNi_{0.5}Mn_{1.5}O_4$ insertion material shows the benefit of having an open structure in which ions can be easily inserted. In that sense the MXene and MoS_2 are more similar to each other with both having open structures. What is more remarkable is that the two cells with the surface-active redox materials, b) and c) both use aqueous electrolytes resulting in narrow operating potential windows of 1.5 V and 1 V compared to 3.5 V of the MoS_2 cell. If the same capacity could be obtained for RuO_2 and MXenes in a non-aqueous electrolyte, it would further boost the energy content of a full cell.

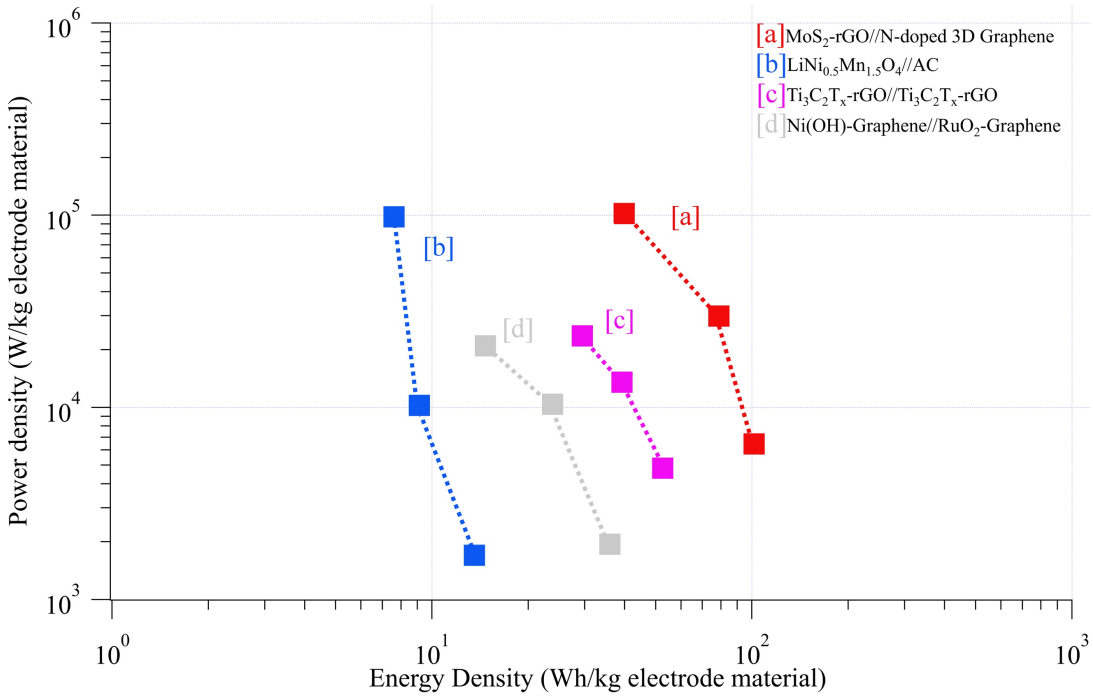

Figure 4. Ragone-plot of four different cells with insertion materials: a) 'MoS_2-rGO//N-doped 3D Graphene' [47], b) $LiNi_{0.5}Mn_{1.5}O_4$//AC [35] and surface-active redox materials: c) symmetric $Ti_3C_2T_x$-rGO [48] and d) Ni(OH)-graphene//RuO_2-graphene [49]

The investigation of charge storage mechanisms of faradaic materials in non-traditional electrolytes has been the focus of this thesis. To optimize the capacity of the electrode materials in different electrolytes it is important to understand the charge storage mechanism of the material and how it is affected by different parameters. MnO_2 has been regarded as a promising material due to the high theoretical capacity and cost efficiency and has been studied extensively. TiO_2 is a well research material for high-power battery anodes [50], and supercapacitors [51]. There is however an issue with an initial capacity fade that is reported extensively for various polymorphs of TiO_2 [52,53]. The capacity fade is attributed to the formation of and entrapment of Li-ions in the structure of TiO_2 [54]. TiO_2 has an intrinsically high electrical conductivity which is important for supercapacitors. At the same time doping of TiO_2-materials have been used as a way to further increase the conductivity for various electrode applications [55], but systematic studies are missing.

3. Charge storage mechanisms

In this chapter, the three dominating charge storage mechanisms in research and in commercial devices are introduced and their advantages and drawbacks discussed. The three charge storage mechanisms are: double layer formation, surface active redox reactions and insertion or battery type materials. There is a fourth type of charge storage mechanism that is out of the scope of this thesis but worth mentioning: Redox-active electrolytes. In this approach the active material is dissolved in the electrolyte and can react when it is next to the electrode surface. It is a promising approach and the charge storage mechanism is similar to that of faradaic electrodes, but with the faradaic component in the electrode dissolved in the electrolyte.[56]

3.1 Double Layer Charge Storage

When electrons are extracted or inserted into an electrode in contact with an electrolyte containing ions, a charged layer will be created inside the electrode. To compensate this, layers of ions will form on the electrode surface in the electrolyte, screening the electrode surface. The structure of the layers will depend on the electrolyte and charge of the electrode. If the electrode surface is assumed to be flat and solid and in contact with a common electrolyte, a salt dissolved in a solvent, three different models have been suggested, Figure 5.

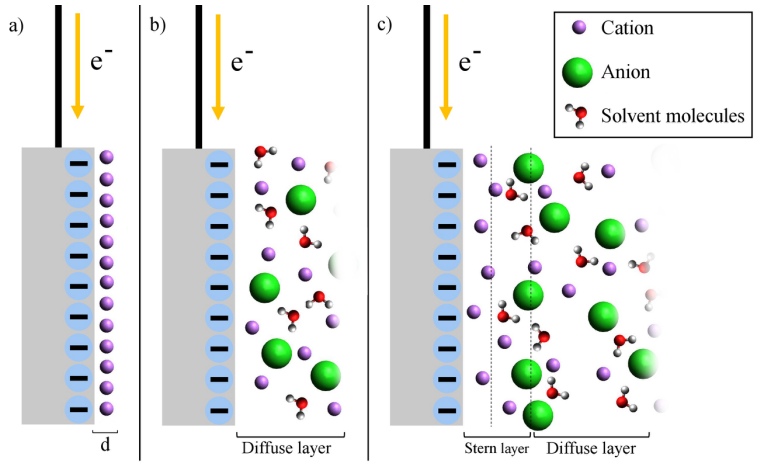

Figure 5. Three different models used to describe the double layer a) Helmholtz model, b) Guoy-Chapman model and c) Stern model

The first attempt to model the electrode/electrolyte interface was made by Hermann von Helmholtz [57] and his model is illustrated in Figure 1a. It is a simple model where the charge at the surface is screened by a compact, rigid, layer of ions with the opposite charge at a certain distance. However, this model is not able to describe experimental observations correctly since no rigid charges exist and it also predicts a constant potential. To better explain the behavior of charged surfaces in an electrolyte Guoy-Chapman suggested the existence of a thicker layer of ions not rigidly adsorbed to the surface [58]. This layer, referred to as a diffuse layer, will screen the surface but contains both positively and negatively charged ions. Even though it is a better model than the Helmholtz model, since it for example considers that the capacitance will vary with the potential, it tends to overestimate the ionic concentration close to a charged surface. As a further modification the Stern model in Figure 5c suggests a combination of the Helmholtz and Gouy-Chapman models, where both a compact inner layer and a more diffuse outer layer screen the charges of the surface [58]. This is the most accurate model and it provides accurate capacitances for flat surfaces.

One issue with all three models is that they can only be used to explain the behavior in traditional electrolytes but not in novel systems, such as ionic liquids [59]. In an ionic liquid the structure of the double layer is suggested to form different structures depending on the potential of the surface [60]. At lower potentials a monolayer of ions will form at the surface, this layer overscreens the surface and is compensated by a second layer consisting of oppositely charged ions. At higher potentials two layers are formed at the surface which dominates the overscreening and a third layer of ions with opposite charge is formed to these [60,61]. A schematic figure of these models can be seen in Figure 6. However, the structure of the double layer in ILs depends on the properties of the ions. There are examples where double layer structures without crowding has been reported [62]. There are also additional models for highly concentrated aqueous electrolytes, that take into account the water distribution in double layers which in these systems plays an important role for the electrochemical stability [63].

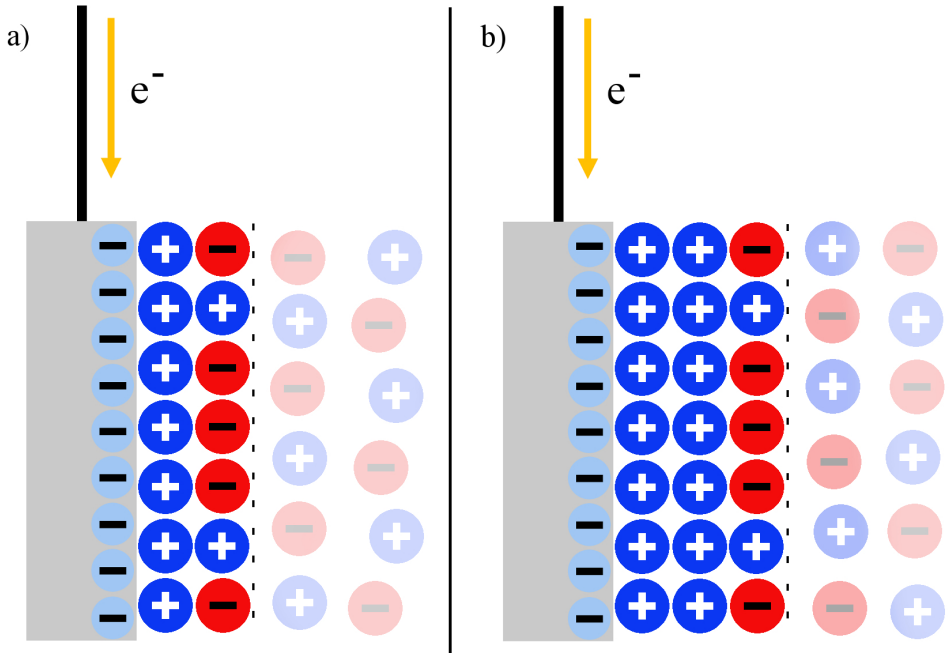

Figure 6. Schematic of two models of double layers in ionic liquids at different potentials. a) Overscreening model at lower potentials and b) crowding model at higher potentials.

Regardless of the electrolyte, double layer structures can be formed and modified rather quickly compared to other electrochemical charge storage mechanisms [58,64]. This means that an electrode relying on double layer charge storage can be charged and discharged very fast and since no reactions are occurring between the electrode and electrolyte, almost infinite cycle lifetime can be achieved. The quick formation of the double layer also has a negative consequence that the double layer structures in the electrolyte is not stable over an extended time and will self-discharge relatively fast. By using different mixtures of electrolytes, the operating temperature of a single device relying on double layer formation can be very wide, ranging from -50 to 80°C [65], in which other energy storage devices will not be able to operate.

The amount of charge that can be stored with the double layer mechanism is also relatively low compared to other charge storage mechanisms [8]. The amount of charge stored directly affects the energy content of the device and leads to a lower overall energy content. The amount of charge, C, that can be stored in double layer structures can be calculated by

$$C = \frac{\varepsilon_r \varepsilon_0 A}{d} \quad (6)$$

where ε is the electrical permittivity of the electrolyte, d thickness of the double layer and A the surface area of the electrode. Of these different properties, the surface area of the electrode is easiest to control to increase the stored charge.

One important exception to consider for both Eq. 6, and the models in Figure 5, is that they only explain the behavior of flat surfaces in electrolytes. Electrodes used in supercapacitors today are porous with different pore-size distributions, which affects the ion transport and charge storage inside the pores. How the pore-size and distribution affect the behavior and charge storage is not completely understood today [66,67]. The pore-size seems to affect the charge storage when it approaches the size of the molecules in the electrolyte. The pore size of a material will also influence the specific surface area of a material, smaller pores results in a larger surfacer area while larger pores will reduce the surface area for a given volume. This means that when increasing the surface area beyond a certain point the, the access to the surface is restricted for larger ions, and charge increase is limited. The general trend however is that the total charge storage will increase with increasing surface area.

The most commonly used electrode material for double layer charge storage is activated carbon. Activated carbon has several benefits, a high specific surface area, up to 4000 m^2/g, low cost and high electrical conductivity [29]. Some examples of specific energy and power densities achieved with symmetric carbon-carbon configurations are 55 Wh/kg – 10 kW/kg using carbon of a coconut precursor [68] and 35 Wh/kg – 3.5 kW/kg using a rice bran pre-cursor [69]. A consequence of maximizing the surface area is that the total pore volume also increases which leads to a lower density of the electrode. Thus, a high surface area carbon material can have relatively high specific gravimetric capacity, but at the same time very low specific volumetric capacity, resulting in a light but bulky device.

3.2 Surface active redox mechanism

This mechanism is confined, like the double layer, to the surface of the electrode material, but for redox reactions to occur electrons need to be transferred between the electrode and the electrolyte. In the electrochemical redox reaction referred to here, the reaction is triggered by a change in the electronic structure of an atom when the potential of the electrode is changed. Different metal oxides are normally used for this type of applications, for example RuO_2 and MnO_2 were the two first materials investigated as redox active electrode materials in supercapacitors [30,70]. However, there are also conducting polymers, such as PEDOT, that possess the same properties [71].

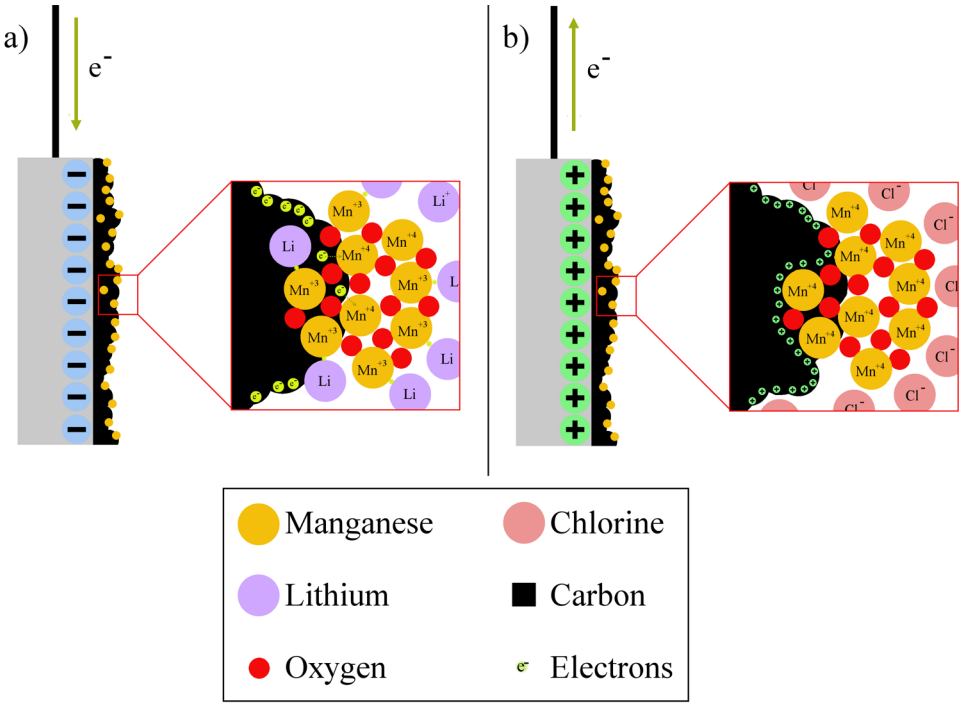

Figure 7. Schematic of a MnO_2-nanoparticle on a carbon support during a) reduction and b) oxidation.

To look into the surface-active redox mechanism in more detail, the charge storage process of MnO_2, in an Li^+ containing electrolyte will be used as example and is illustrated schematically in Figure 7.When the potential of the MnO_2 electrode is lowered and electrons flow into the electrode, the Mn-atom will absorb an electron, reducing its oxidation state from Mn^{+4} to Mn^{+3} and at the same time it will form a so-called solid solution with the Li-ion in the electrolyte to compensate for the change [31,72]. In Figure 7b the current is reversed, the potential is increased and electrons are stripped from the electrode. This will reverse the oxidation from Mn^{+3} to Mn^{+4} and Li^+ will dissociate into the electrolyte at the same time a double layer will be formed at the surface consisting of negatively charged ions. This redox reaction can be summarized as [73]

$$(Mn(IV)O_2)_{surface} + Li^+ + e^- \leftrightarrow (Mn(III)OOLi)_{surface} \quad (7)$$

In aqueous electrolytes the charge storage mechanism has been explained by the interaction between the MnO_2 surface and alkali metal cations combined with protons [73], even in alkaline aqueous electrolytes [74]. This explains why the obtained charge storage is generally higher for MnO_2 in aqueous than organic electrolytes [8,75] where no protons are available. This is contradicted to some extent by research on MnO_2 in ionic liquid electrolytes that has shown that MnO_2 materials can interact directly with aprotic IL-cations [76] and anions [77]. More in line with the charge storage mechanism in aqueous electrolytes, are results presented for protic ILs where an excess of protons enables a larger faradaic charge storage similar to that in neutral aqueous electrolytes [78]. However, the difference in interaction of protic ILs, where protons are available but not in excess, and aprotic ILs have not been studied previously.

The charge stored in redox reactions is proportional to the number of electrons transferred which depends on the actual electrochemical reaction and the number of active atoms in contact with the electrolyte. The number of electrons taking part in the electrochemical reaction is equal to the change in oxidation number. The number of available oxidation states depends both on

the electronic structure of the material and the electrolyte composition. While MnO_2 only has two available oxidation states in aqueous electrolytes, V_2O_5 has been found to have up to 3 oxidation states available [79]. However, when changing the oxidation state, the local structure in the material also changes. These changes can lead to unwanted side-effects such as irreversibly reduced redox activity and dissolution of active material which is the case for MnO_2 when the potential is lowered too much [72].

Another important drawback of most metal oxides is that the electrical conductivity is low compared to activated carbon, which is especially problematic for high-power charge storage. To reduce the resistance in the electrodes, the layers or particles of active materials should be kept very small and thin, within a couple of nanometers if possible. The reduction of particle size has also the beneficial effect that the surface area increases and the number of active atoms interacting with the electrolyte will increase. If the particles are sufficiently small most atoms will be at the surface and the charge storage will compete with that of insertion materials discussed further below. The electrical resistance of metal oxides can also be reduced by tuning the electronic structure of the material, by doping the material with different atoms [80,81] or by creating deficiencies in the structure which can potentially increase the conductivity [82].

Some examples of energy and power densities achieved for different hybrid electrode setups using surface active redox materials is around 8 Wh/kg - 20 kW/kg for MnO_2/CNF [83], 31 Wh/kg - 9.5 kW/kg for TiO_2/AC [84] and 43.4 Wh/kg - 7.5 kW/kg for Nb_2O_5/AC [85].

3.3 Insertion type materials

Double layer and surface-active redox-reactions are both mechanisms that only utilize the surface of the electrode for charge storage. This leads to a large fraction of the electrode being unused. In insertion-type materials, or battery type materials, the charge storage is based on insertion and extraction of ions into the bulk of the active material [86]. Compared to the surface-active redox mechanism, the insertion/extraction charge storage mechanism is often more complex. During insertion of ions the structure, as well as physical properties such as electrical conductivity and density of the material, can change as the inserted ions become part of the host structure. There might also be several different phases of the same material present at the same time with different properties. Generally, the higher the capacity of a material, the more complicated reactions and slower reaction kinetics come as a consequence. This can be explained by the large number of ions that need to be inserted into the material to achieve a high-capacity. For example, in silicon which has a theoretical capacity of 4200 mAh/g, the structure undergoes a phase change from a crystalline to amorphous phase upon the insertion of 3.75 Li-ions/Si atom[87], this leads to a large strain on the material due to the volume expansion/contraction and as a consequence, fast capacity fade due to cracking of particles. These types of materials are predominantly used in batteries due to their high capacity. A more suitable insertion material for supercapacitors is TiO_2 which has a high Li-diffusion [88] and a modest reversible Li-insertion limit of one 1 Li / TiO_2 [89]. Despite being more suitable for supercapacitors there are several other undesirable processes that can occur in insertion materials, some of which are schematically shown in Figure 8.

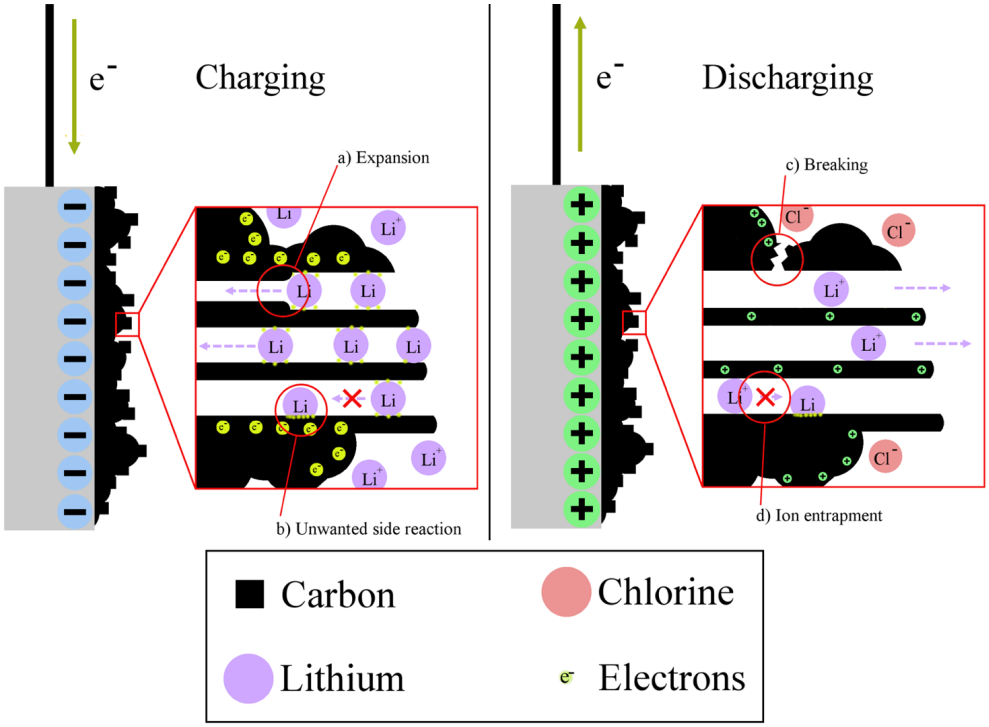

Figure 8. Schematic of an insertion and extraction process indicating some common problems, a) Expansion, b) Unwanted side-reactions or parasitic reactions, c) Breaking of the material and d) ion entrapment in the material.

The limiting factor during charging and discharging of insertion type materials is normally the ion diffusion in the electrode. This is opposite to the formation of double layers and surface-active redox materials where the electron transport is the limiting factor. At high-power the charge stored in insertion-type materials will be lower and the strain on the material will limit the cycle lifetime [90]. However, there are a number of ways to mitigate these issues and improve the high-power performance: By improving the ion diffusion in the material it is possible to increase the number of ions inserted during high-power operation. This can be achieved by for example nanosizing the particles of active material in the electrode. Nanosizing the particles will also increase the fraction of charge stored at surface sites [91], and can also reduce the effect of structural changes that occur in the material [92]. Embedding the particles in a porous, conducting material is also important to enable the electrolyte to infiltrate the electrode and access the nanoparticles in the electrode. Examples of specific power and energy obtained from electrode setups that use insertion type materials are 15 Wh/kg at 2.5 kW/kg for AC/$Li_4Ti_5O_{12}$ [93] and 40 Wh/kg and 10 kW/kg for a AC/Graphite electrode setup [94].

Another approach is to use materials where the bulk and surface is not differentiated. One such type of material that has received considerable attention lately are so-called MXenes. MXenes consist of layers, atomically thin sheets of atoms, and can be built up of a many different atomic species [95]. Due to the fast insertion of ions in between the sheets and the subsequent fast redox-reactions very promising results have been obtained [95]. For example, a capacitance of 335 F/g, corresponding to capacity of 87.5 mAh/g at 100 mV/s, has been obtained for a composite electrode consisting of the MXene $Ti_3C_2T_x$ [96]. The redox reactions occur during both reduction and oxidation which makes it possible to use it both as a negative and positive electrode. What is even more remarkable is the ability to maintain 60 % of the capacitance at the extremely high scan speed of up to 1 V/s. These properties combined with the high density of the material has been demonstrated in a symmetric device with an energy density of 3.3

Wh/kg at 24 kW/kg power density [48]. However, MXenes have mostly been used in strongly acidic aqueous electrolytes and further studies are required to transition to more electrochemically stable electrolytes which could improve the energy content even further.

3.4 Charge storage in practice

In the discussions about the different charge storage mechanism above it is easy to envision that electrodes only can possess one of these charge storage mechanisms. However, by modifying the materials, the charge storage can be more of a blend between two or more mechanisms. For example, by introducing the layered $Ni(OH)_2$-$Co(OH)_2$ structure, with easier Li-insertion a higher contribution from faradaic reactions can be obtained compared to the $Co(OH)_2$ were a larger fraction will come from double layer formation [97]. As mentioned previously, activated carbon electrodes rely almost only on double layer charge storage, however, it is important to take into consideration that double layers contribute to the total charge also in electrodes that rely on other charge storage mechanisms. The fraction from double layer charge storage increases with faster charge/discharge times are of importance at high-power conditions. This behavior is illustrated by Sugimoto et al for a RuO_2 material where the double layer capacitance dominates completely at 100 mV/s [6]

4. Electrolytes

If the electrodes are the muscles of a supercapacitor, then the electrolyte is the nervous system that connects the part and makes it work. In the research on new electrode materials for supercapacitors, a majority of the studies use aqueous electrolytes for the electrochemical characterization and performance measurements [8]. Aqueous electrolytes can have pH-values ranging between very acidic to strongly alkaline, depending on the choice of salt used. Aqueous electrolytes have high ionic conductivity, e.g. up to 730 mS/cm for alkaline electrolytes and 800 mS/cm for acid electrolytes [98], which is more than one order of magnitude higher than what can be achieved in non-aqueous electrolytes [99]. The high conductivity ensures that the performance and behaviour of an electrode is not limited by slow kinetics of the electrolyte. The use of aqueous electrolytes also makes it easier for researchers to compare electrode results and behaviour since the use of aqueous electrolytes is almost standardized [8]. Aqueous electrolytes are also easy to handle and require no additional lab-equipment for measurements.

There are, however, also several drawbacks related to aqueous electrolytes. The most significant is the narrow electrochemical window, limited by hydrogen evolution at 0 V vs. SHE and oxygen evolution at 1.23 V vs. SHE [8]. The pH of the electrolyte affects the width of the stability window, with narrower stability windows for acidic and alkaline electrolytes [100]. The small stability window limits the energy and power density of the full device, since it is directly proportional to the voltage window, see Eq. 3 and 4. Another drawback of alkaline and acidic electrolytes is their severe corrosivity which might make them unsuitable for some applications.

When developing new materials for supercapacitor applications, the interaction with the electrolyte is important to consider. If the development is done primarily with aqueous electrolytes it is not certain that the new material has the optimal structure and characteristics for more electrochemically stable electrolytes [101,102]. For example, carbon materials have a certain pore size distribution and narrow pores and high surface area might be suitable for aqueous electrolytes with small ions, while non-aqueous electrolytes might require larger pores [103] and a lower surface area for high performance. This is only one example where the difference between aqueous and non-aqueous electrolytes should be taken into consideration.

In a majority of EDLC devices on the market organic electrolytes are used [2]. This is due to the larger potential window of organic solvents which increases the energy density of the device while maintaining a reasonable high-power performance. The organic electrolytes are usually based on acetonitrile or mixtures of organic solvents similar to electrolytes used in batteries [2,86]. Besides the increased electrochemical stability, they are also quite cost-effective which is important for the supercapacitor industry where an upper cost limit of 12 EUR/kg electrolyte has been suggested for future devices [2]. The biggest drawback is probably the safety concern, electrolytes based on organic solvents are normally very flammable compared to aqueous electrolytes. Some examples of electrolytes are given in Table 1

Table 1. Some examples of electrolytes used in research on supercapacitor materials and in commercial devices.

Solvent	Salt	Potential window	Conductivity (mS/cm)	Ref.
Acetonitrile	TEA BF_4	2.8 V	55 (1 M)	[26]
Propylene carbonate	TEA BF_4	2.9 V	13 (1 M)	[104]
ethylene carbonate dimethyl carbonate (1:1)	LiTFSI	1.8 V	11 (1 M)	[105]
Water	KOH	0.73 V	730 (6 M)	[3]
Water	Na_2SO4	1 V	120 (2 M)	[106]

Two new electrolyte concepts that have gained increased research interest during the last couple of years, in an effort to mitigate some of the issues of aqueous and organic electrolytes, are ionic liquids (ILs) and highly concentrated electrolytes (HCE). In the following two parts these two concepts will be discussed more in depth and previous research using these electrolytes will be presented.

The electrolytes described in this chapter as well as used in this thesis work are all liquids. However, there are examples of different solid electrolytes for supercapacitor applications but they are outside the scope of this thesis [107].

4.1 Highly-concentrated Electrolytes

In aqueous electrolytes the electrochemical stability is limited by the decomposition of water at the electrodes. Water molecules in an aqueous electrolyte containing an alkali metal salt interact and coordinate with the alkali metal cations [108]. By increasing the salt concentration, a larger fraction of the water molecules will be coordinating the metal cations which leads to an increase in the overall oxidative stability of the electrolyte and a preferential reduction of the anion [10,109]. However, the common salts used in neutral aqueous electrolytes today, such as Na_2SO_4, have a solubility limit around 1.1 m [110] which is not enough. There are however a range of so-called weakly-coordinating salts, with which it is possible to reach very high concentrations.

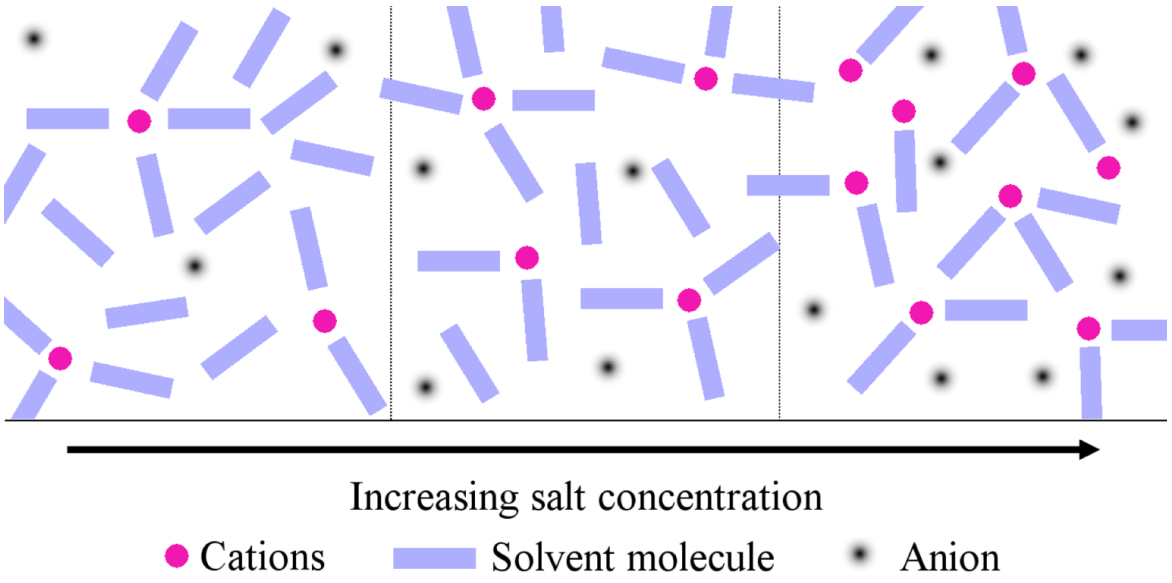

Figure 9. Schematic electrolyte structure with increasing salt concentration.

The first major publication on an HCE electrolyte for battery applications was Suo et al, who showed the expanded electrochemical stability window of a 21 m LiTFSI aqueous electrolyte [111]. They show that by increasing the salt concentration a majority of the water molecules is coordinated to the Li-ions. This leads to a situation where the TFSI anion is in contact with the electrode during cycling, instead of the water molecules [27], and that a so-called solid electrolyte interphase layer is formed in this potential window. Generally, for supercapacitors this is detrimental since it would increase the charge-transfer resistance of the electrode. A schematic illustration of the development of the coordination in an electrolyte as a function of salt concentration is shown in Figure 9.

Another drawback is that the conductivity is drastically reduced at high concentrations. In a 21 m aqueous LiTFSI electrolyte it only reaches around 9 mS/cm [27]. The 21m LiTFSI electrolyte has been used together with a MnO_2 electrode with a wider potential window as a result [112]. However, already at moderate concentrations (>5 m) [27] the electrolyte can be described as a water-in-salt system where most of the water molecules are coordinating with cations as discussed earlier. This was later expanded to other systems with other salts and solvents [113]. One example is by lowering the concentration of the highly-concentrated aqueous electrolyte and replacing the LiTFSI with NaTFSI, 8 m NaTFSI in water has been tested as a middle road with high conductivity and increased electrochemical stability window compared to other aqueous electrolytes [10]. Highly concentrated aqueous electrolytes containing salts with other, more common anions, have also been investigated such as 5 M $NaClO_4$ [114] and saturated $LiNO_3$ [115] but without the increase in stability window compared to the electrolytes containing salts with the TFSI anion. This shows that the anions also need to have the ability to block the electrode and be stable to electrochemical reduction and oxidation to increase the electrochemical stability window.

Moving away from water based electrolytes, acetonitrile, which is very popular for supercapacitor applications, has been shown to have a very wide electrochemical stability window at 4.2 M LiTFSI concentration [116]. However, the conductivity of the electrolyte was barely 1 mS/cm, so it was not so suitable for supercapacitor applications. An interesting hybrid between highly concentrated aqueous and organic electrolytes is a so-called ‘acetonitrile/water in salt’ electrolyte suggested by Dou et al [117]. In this concept water and acetonitrile are mixed and the capacitance is enhanced compared to when using the 21 m LiTFSI electrolyte in a 2 V potential window for a symmetric carbon/carbon cell [117].

4.2 Ionic Liquid Electrolytes

Most salts are solids at room temperature, having melting temperatures of several hundred degrees celsius. ILs are salts, i.e. consist only of ions, but are liquid at room temperature. The ions in ILs are considerably bigger and more flexible compared to ions in conventional salts. By increasing the size of the ions, the melting temperature generally drops due to the reduced ion-ion interaction. Sterically hindered ions prevents the IL from crystallizing, asymmetries in the ion structure and conformational flexibility further promotes a low melting temperature [118,119]. The viscosity follows approximately the same trend as the melting temperature, but when the side-chains of the ions become longer the contribution from the Van der Waals forces increases the viscosity of the IL [118].

For energy storage applications important properties of electrolytes are high conductivity, electrochemical stability, non-flammability, low viscosity. All of these properties can, to some extent, be realized in ionic liquids, making ILs promising electrolytes and/or solvents for electrochemical storage applications [120]. An additional property of ILs is the non-existing

vapour pressure and high temperature stability which makes IL electrolytes suitable for high-temperature applications [121]. The ions can be tailored almost infinitely [122] making it possible to adapt a certain ILs to different applications.

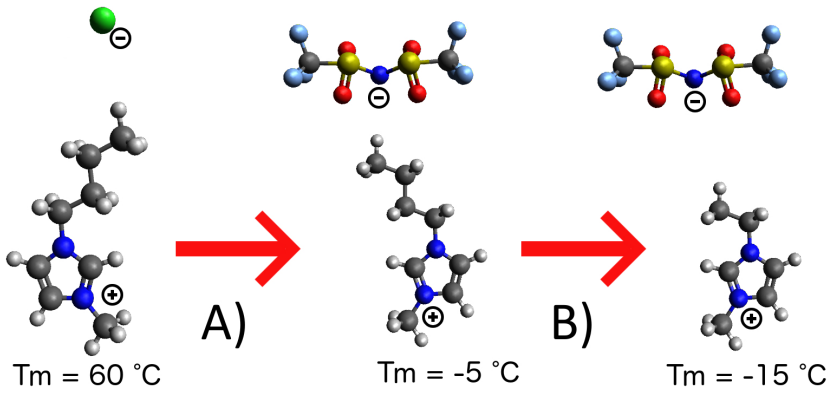

Figure 10. Example of how the structure of the ions affect the properties of BMIM Cl (left), BMIM TFSI (middle) and EMIM TFSI (right).

An example of how different structures affect the properties of ionic liquids is shown in Figure 10. The IL to the left in Figure 16 has a melting point of around 60 °C, this makes it unsuitable for most electrolyte application at room temperature. By changing the chloride anion to the bigger TFSI anion in step A the melting point is reduced to -5 °C, making it a liquid at room temperature. However, this IL has a high viscosity and low conductivity, 61 cP and 4 mS/cm [123] at 25 °C respectively. To further improve the physical properties, the cation is made slightly smaller in step B) which reduces the viscosity to 35 cP and the conductivity is increased to around 8 mS/cm [123]. However, the maximum ionic conductivity achieved for an IL at room temperature is around 15 mS/cm [120], which is low compared to the aqueous and acetonitrile based electrolytes, see Table 1. The viscosity is also higher, 18-62 mPas for the most promising ILs compared to the viscosity of TEA BF_4/ACN of 0.6 mPas [26].

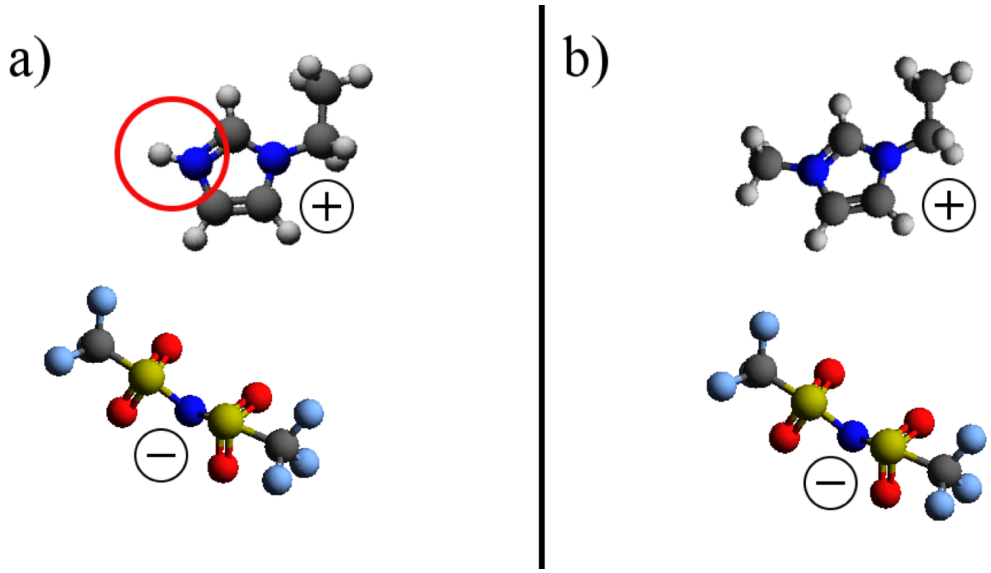

Figure 11. Examples of a) a protic IL EIM TFSI with the loosely bound proton marked and b) an aprotic IL EMIM TFSI.

ILs can generally be divided into two categories: protic and aprotic. The difference between these categories is in the availability of protons in the ionic structure. This is linked to the ability of the ion to form hydrogen bonds and even donate protons in chemical reactions [124]. A comparison of a protic and aprotic IL is illustrated in Figure 17 where IL in Figure 17a has a proton loosely bound to the nitrogen in the imidazolium ring compared to the protons in the aprotic IL in Figure 17b that are strongly bonded to carbons. However, this change in structure will also affect the electrochemical stability, as discussed previously. The hydrogen bound to the nitrogen will be sensitive to reduction thus reducing the electrochemical stability window of the IL from 4.1 V for the aprotic IL to 2.5 V for the protic IL [125].

The loose proton in the protic IL is formed through proton transfer from a strong acid to a strong base during the synthesis [124]. However, there are also aprotic ionic liquids that potentially have the ability to form hydrogen bonds, so called Brønsted-acid ILs. In the synthesis of these ILs no proton is transferred, instead they have one or more functional group attached to either the cation or the anion, that has a hydrogen-bond forming ability [124]. This is achieved by having a proton attached to an electronegative atom, such as oxygen or sulfur, which gives it the similar hydrogen bond forming ability as molecules such as water or ethanol. An example of a Brønsted-acid IL is shown in Figure 12 with the hydrogen-bond forming proton marked.

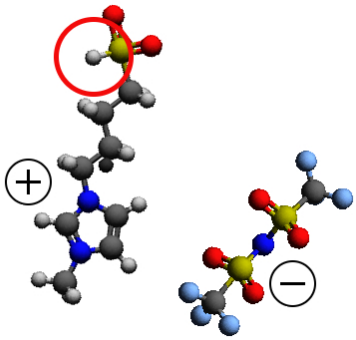

Figure 12. An example of the quite acid Brønsted-acid SBIM TFSI.

Despite the low conductivity of ILs, there is an interest in the supercapacitor community to exploit them for supercapacitor applications. Aprotic ILs are most commonly investigate due to their low water-uptake and limited chemical interaction with the electrodes. Research on EDLC devices using neat ILs as electrolytes have shown a high capacitance of graphene based carbon materials, 270 F/g, by using 1-ethyl-3-methylimidazolium tetrafluoroborate as electrolyte in a device with a 4 V operating voltage outperforming a cell with the same electrode material but using a standard organic electrolyte in both power and energy density [126]. Another example is the use EMIM TFSI showing identical performance as a standard organic electrolyte with activated carbon electrodes [127]. Some results from an extensive study [128] on various ILs used in symmetric cells with carbon nanotube-based electrodes are presented in Table 2. The results demonstrate the possibility of devices with increased energy density by using neat ILs, but high-viscosity limits the power density.

Table 2. Summary of the potential window, energy and power density obtained for various electrolytes with the same electrode

Electrolyte	Voltage window (V)	Energy density (mWh/cm^3)	Power density (W/m^3)
ACN/TEA BF_4	2.7	12	930
DEME BF4	4.7	41	155
PYR14 TFSI	4.3	39	375

To mitigate the negative effects of high viscosity and low conductivity of ILs they can be mixed with an appropriate solvent. Jänes et al showed that by adding 1,2-dimethoxyethane to the EMIMTFSI the conductivity increased with a factor 4 which resulted in the power density from 13 to 20 kW/kg of a symmetric titanium derived carbon cell at a constant energy density [129]. The high temperature stability of ionic liquids has shown that operation at up to 100 °C using microporous carbons [130] as well as the feasibility of using the ionic liquid 1-Ethyl-3-methylimidazolium acetate in the temperature range 21 – 100 °C with an improved capacitance from at a scan speed of 500 mV/s and reduced resistance of the cell as an effect of the increased temperature [131].

Examples of studies on IL based electrolytes together with insertion type electrodes have been published. For example, a $LiMnO_4$ electrode in a 0.5 M LiTFSI/EMIMTFSI electrolyte resulted in relatively low power and energy density [132]. In this example, the IL is used as a solvent or a double layer forming salt and the Li-ions interact with the electrode material enabling a faradaic contribution to the total capacity.

There is also another approach that has been considered. Since materials such as MnO_2 and RuO_2 have been shown to undergo redox-reactions with protons in aqueous electrolytes, this could potentially also occur in certain ionic liquids. By using redox materials in protic and Brønsted-acidic ILs it could be possible to achieve a faradaic contribution from the redox-active material while increasing the potential window of the device. ILs with protons loosely bound to the ions will have a narrower electrochemical stability window of 2-2.5 V for imidazolium based protic ILs [125] but up to 3.9 V for the Et3NHTFSI IL [133] which is close to the 4 V reported for the frequently used aprotic EMIMTFSI IL. There have been some results reported on protic ILs as electrolytes for various applications such as batteries [133] where it is used as a solvent and in EDLC setups and showing good cycling stability and no faradaic interaction with the carbon material [134]. Another study the pyrrolidinium nitrate ionic liquid was cycled in a voltage window of 1.2 V in a two electrode setup. The results in this study showed interaction with the carbon electrode [135]. In other studies on redox-active electrodes, a protic IL has been shown to interact directly with RuO_2 material in a similar way like an aqueous H_2SO_4 electrolyte and no interaction from the aprotic IL [136]. In a third study a MnO_2-thin film electrode showed a similar behaviour which was associated to a proton exchange with the material [78].

Finally, as mentioned previously there are almost unlimited choices when it comes to the design of ILs. A tempting idea would be to make ILs consisting of ions that can undergo redox reactions while in solution. There are a few studies worth mentioning in which the ILs themselves contribute to the charge storage by undergoing redox-reactions. One example is attaching a ferrocene group on the anion [137] in which the ferrocene responded to the potential change with very high reversibility up to 1 V/s. Also other complex IL based electrolytes where redox-active groups on both ions further have shown increased capacity of full cells with good cycling stability [138].

5. Experimental techniques

Several different methods have been used to characterize the materials and their electrochemical behavior in different electrolytes in this thesis. The most important methods, their strengths and drawbacks, are presented in this chapter.

5.1 Cell setup

Two different experimental setups are used for most electrochemical measurements: 3- and 2-electrode cells. In electrochemical measurements three different components are generally required:

- The working electrode (WE): The electrode investigated in the experiment.
- Reference electrode (RE): Consists normally of a well known redox couple to which the potential is measured against and determines the position of the experimental potential in the electrochemical landscape.
- Counter electrode (CE): The CE balances the WE, for every electron that is transferred to, or from, the WE the opposite electron transfer process needs to take place at the CE.

In an electrochemical experiment the electrical potential will drive the electrochemical reactions. Thus, to be able to understand the behavior of a system an accurate measurement of the potential is required. However, the potential is not measured on an absolute scale, but is always measured against a known redox couple. The purpose of the reference electrode is to provide a well-known and controlled potential. This is often achieved by immersing a metal substrate into a solution containing a suitable counter ion. For example, Ag/AgCl is a well known redox couple and is achieved by immersing a silver wire into a saturated, aqueous, KCl solution. The reference electrode, containing the solution and silver wire, is connected with the electrolyte through an ion conducting membrane. By measuring the potential of the WE vs. the reference makes it possible to compare specific measurements with other results in completely different systems. The choice of reference is normally not a problem for aqueous electrolytes. However, for non-aqueous electrolytes this can be more difficult. Their sensitivity to water makes references such as Ag/AgCl reference unsuitable. The solvent in the RE should be the same as the solvent in the electrolyte. For ionic liquids this is difficult to achieve since the ILs might interact with the metallic substrate in the RE.

A common workaround for IL based electrolytes is to use a stable metal foil directly immersed in the electrolyte of the actual experiment as a reference. However, since no suitable counter ion is present in the electrolyte, it is not the potential of the redox reaction that determines the potential of the reference but instead the stripping and plating of metal ions. This approach is not ideal and is not as stable as traditional Res. In literature this type of RE is often referred to as a pseudo or quasireference [139]. The pseudoreference will also have different potentials in different electrolytes therefor it needs to be characterized against a well-known redox couple, eg. Ferrocene/Ferrocenium, before starting the experiment in a particular electrolyte [139]. For the measurements in ILs in this thesis silver-foil was chosen as pseudoreference.

The CE should have a higher surface area than the WE and be inert in the electrolyte to prevent the electrical behavior of the WE to be limited or governed by the CE. The difference between a 2- and a 3-electrode setup lies in how the RE and CE are controlled. They are also used for slightly different purposes i.e.: The 3-electrode setup is used for characterizing individual electrodes and 2-electrode setups are used for characterizing the behavior and performance of

full cells. In a 3-electrode setup the RE and CE are measured separately, ie. the potential of the WE, CE and RE are independent of each other. A schematic figure of a three-electrode setup is shown in Figure 13.

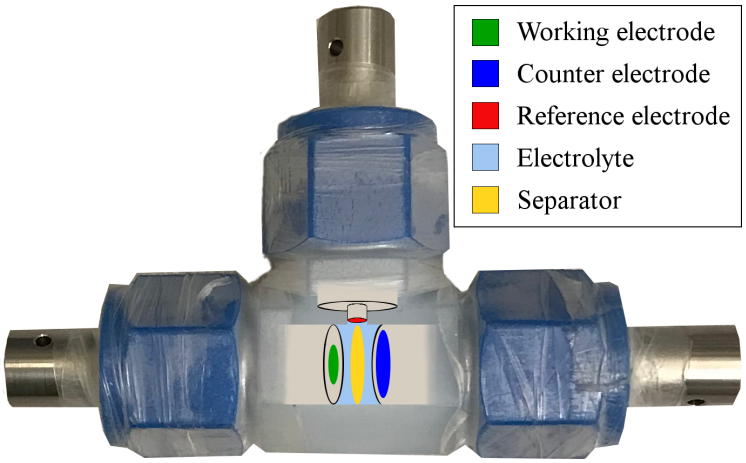

Figure 13. Schematic of a 3-electrode cell used in this thesis. In the actual setup a separator is pressed between the WE and CE.

In a 2-electrode setup the CE and RE are combined into one electrode. Since the CE and RE is the same electrode, the potential of the CE/RE electrode changes simultaneously as the WE. This makes it impossible to know the exact potential of the WE and to compare the results of individual measurements. An exception is if a well known redox couple with excess capacity is used as CE/RE Common examples of such electrodes in battery research are alkali metal foils, such as Li or Na, combined with the corresponding ions in the electrolyte. A schematic figure of a two-electrode setup is shown in Figure 14.

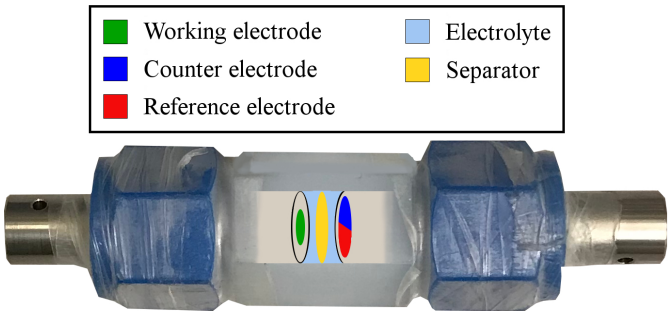

Figure 14. Schematic of a 2-electrode setup, integrating the CE and RE into one electrode.

5.1.2 Electrode preparation

To convert the active electrode material into an actual electrode requires some preparation. If the active material is synthesized as a powder three additional components are necessary to prepare the electrode: current collector, binder and a conductive additive. The conductive agent is normally a carbon material and its purpose is to increase the conductivity of the electrode when poorly conducting active materials are used. The binder is added to bind the components together and ensure good adhesion to the current collector. The electrode is prepared by dissolving the components in a suitable solvent and the slurry is coated onto a current collector, usually a metal foil. This electrode preparation approach was used in **Paper I, II**, **IV**, **V and VI.**

The choice and amount of conductive additive, binder, solvent and current collector is important for the overall electrode performance. In the electrodes prepared in this work the amount of active material was around 70-80 %, and the binder and conductive additive make up equal parts of the remaining 20-30 %. As for the amount of solvent this varies between materials so a trial and error approach with gradually increasing the amount of solvent until a desirable viscosity of the slurry is obtained. Examples of negative impact the non-active material can have is that a poor binder will reduce cycle lifetime and certain current collectors are not stable in all electrolytes and potential windows.

For practical applications the mass loading of the electrode is important. Low mass loading results in thin layers and high specific capacity, but the areal capacity and in extension the energy and power density of the device, will be too low to be useful for real applications. Electrodes in commercial supercapacitors generally have about 10 mg/cm^2 [140], this can be compared to the mass loading of about 5 mg/cm^2 in **Paper II**. In the other papers the mass loading was a bit lower, around 3 mg/cm^2.

If the electrode can be synthesized into a self-standing structure this omits the need of a current collector. This can be achieved by using for instance interconnecting matrixes of carbon nanofibers that will be mechanically flexible and have a high electrical conductivity. This can be beneficial from both a cost and performance perspective, self-standing electrodes were used in **Paper III.** A comparison of a self-standing electrode and a traditional current collector electrode with a Cu-foil demonstrated is shown in Figure 15.

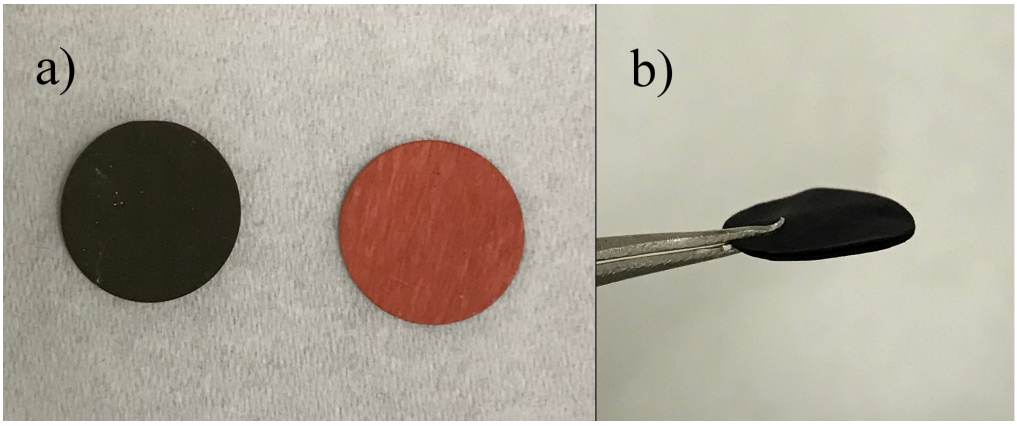

Figure 15. a) A traditional electrode coated on a Cu-foil current collector and b) a self-standing CNF electrode.

5.2 Cyclic voltammetry

In cyclic voltammetry (CV) the potential of the cell is changed at a constant rate between defined potential limits, and the current is measured. Analyzing a cyclic voltammogram (CV) gives important information on the charge storage mechanism and electrochemical behavior of the material investigated. It can for example answer the scientific questions: Is any charge stored in the material? Are there chemical reactions occurring? And if so, are they reversible?

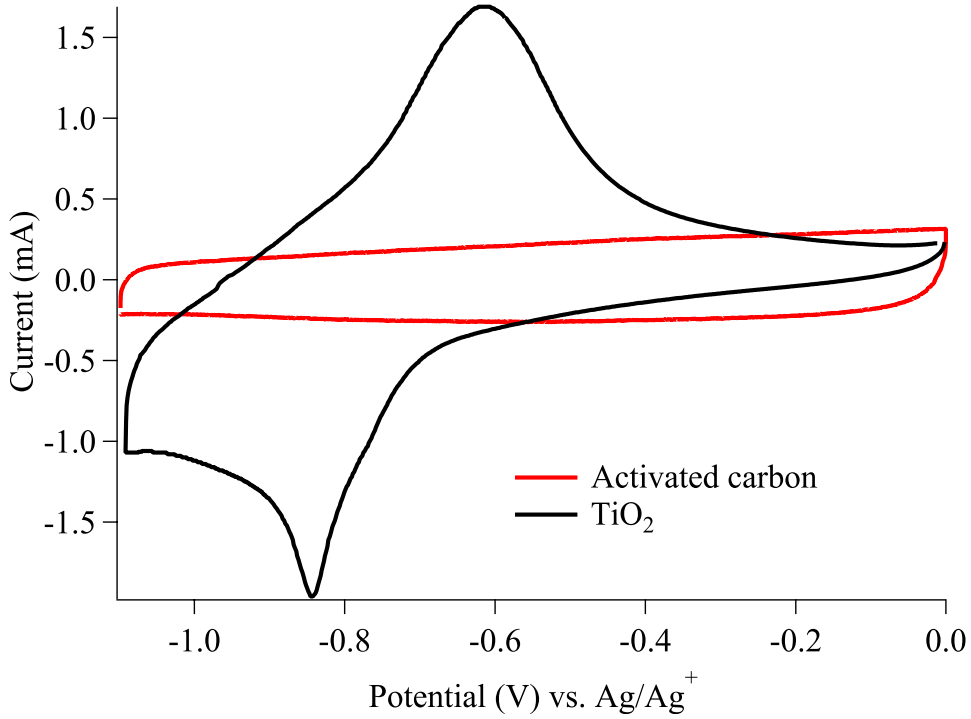

Figure 16. CVs of two different materials with different charge storage mechanisms: activated carbon with double layer charge storage and TiO_2 with faradaic charge storage in an aprotic ionic liquid electrolyte 0.5M LiTFSI/EMIM TFSI for TiO_2 and EMIM TFSI for the activated carbon.

An example of two materials with different charge storage mechanisms is shown in Figure 16 The rectangular shape of the CV from activated carbon is generally interpreted as formation of double layers is the major charge storage mechanism. Double layer formation is a continuous process during the potential change resulting in a constant current as the double layer is formed with the changed potential. The peaks in a CV means that at a certain potential a flow of electrons to or from the electrode will be initiated from electrochemical reactions that start to occur at that potential. This electron flow comes from either oxidation or reduction processes of the active material in the electrode and/or electrolyte species [141,142]. These redox reactions depend on the potential of the electrode, and the curve appears from the saturation and depletion of ions interacting in the redox process in the layer closest to the electrode surface or in the bulk if insertion processes are occurring [141]. Materials with clear peaks in the CV is often referred to faradaic materials in supercapacitor research. One should note that if thin layers of MnO_2 or RuO_2 are used in the electrode, the redox reaction at the surface of these materials will still result in a rectangular CV, similar to the one of double layer formation, but with a larger current response. This behavior is called pseudocapacitance [25].

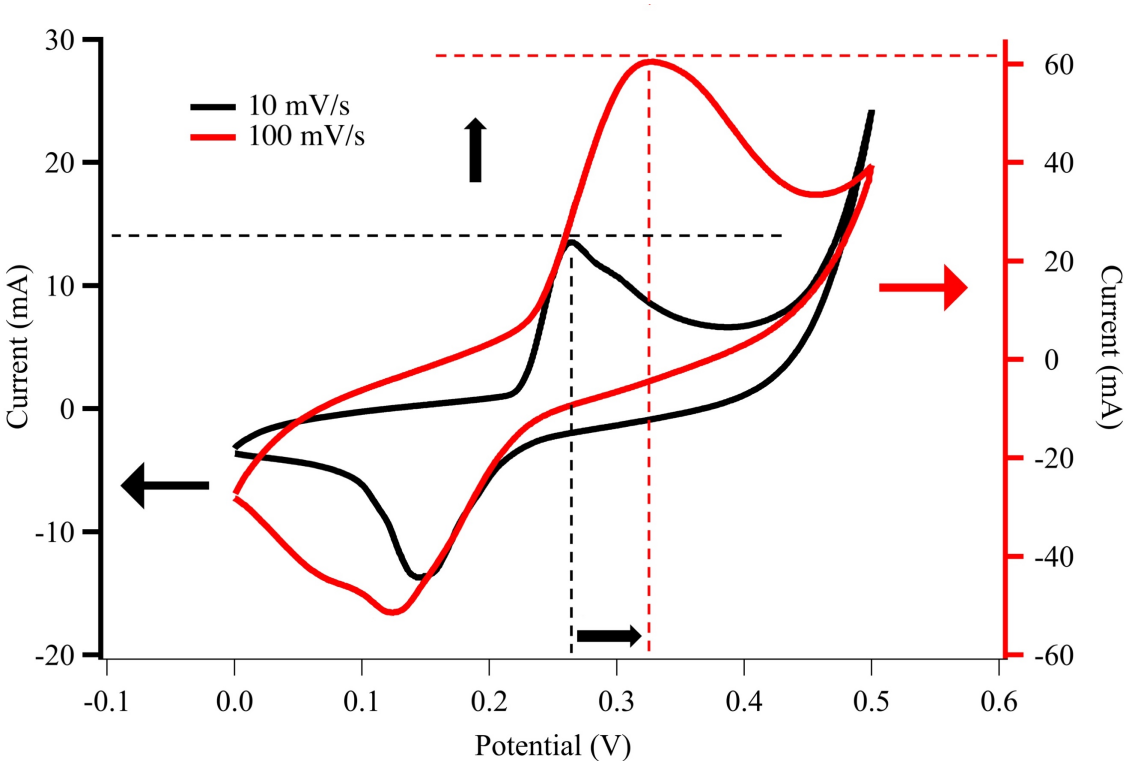

Figure 17. Comparison of the CVs acquired for a VO_2 electrode in a 6 M KOH electrolyte at two different scan speeds, 10 and 100 mV/s.

The current of the peaks and double layer formation depends on the scan speed and increases with increasing scan speed. The width of the individual peaks and peak separation is also increased with increasing scan speed [142]. An example of how the CV of a faradaic material changes with increasing scan speed is shown in Figure 17. The scan speed in a CV experiment is chosen depending on what type of material and mechanism being investigated. Slow scan speeds around 1-5 mV/s are suitable for initial measurements on completely new materials for supercapacitors. If there are electrochemical reactions occurring, the peaks will be sharper and easier to interpret at the slower scan speed. However, to measure and analyze the actual behavior and performance of the system, measurements at higher scan speeds are also important for supercapacitor materials. Careful investigation of the CVs reveals important information about the different properties of the material. For example, if more peaks are visible this indicates that more than one reaction is taking place. A small peak separation and sharp peaks at faster scan speeds indicates a fast charge storage mechanism, which is important for supercapacitor applications. As an example, to compare different charge storage processes in systems with different kinetics and different electrolytes, different systems are compared at the same scan speed in Figure 18. Figure 18a is a CV of a redox reaction of a molecule dissolved in an ionic liquid with relatively low conductivity. The CVs in Figure 18b is from a faradaic metal oxide in a very conducting electrolyte and the CV in Figure 18c is from a different faradaic material in the same IL electrolyte as in Figure 18a. Based on the peak separation in Figure 18, it is possible to say that of these processes the VO_2 electrode in the KOH electrolyte is the shows the fastest kinetics. The ferrocene/ferrocenium couple is slower due to the low conductivity of the electrolyte, in an aqueous electrolyte this separation is considerably smaller [57]. The TiO_2 electrode in the ionic liquid has slower kinetics as a result of slow transport in the electrolyte and since the charge storage mechanism is not limited to the surface.

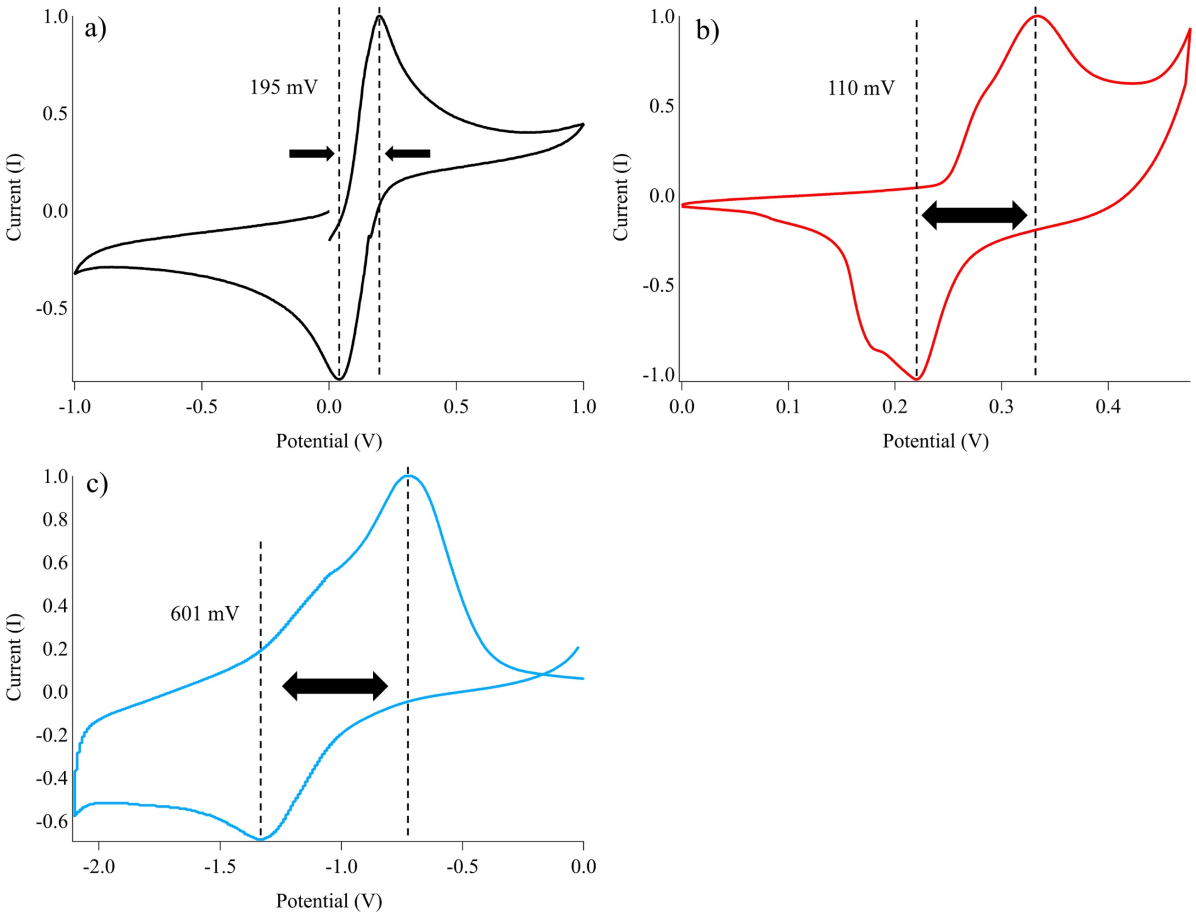

Figure 18. Comparison of the peak separation in three different systems at the same scan speed: a) Ferrocene/Ferrocenium couple dissolved in EMIM TFSI b) VO_2 electrode in a highly conductive 6 M KOH electrolyte and c) a TiO_2 electrode in an 0.5M LiTFSI/EMIM TFSI electrolyte.

Integrating the curve according to Eq. 8 will provide the amount of charge stored at a certain scan speed, i.e. the specific capacity at that scan speed [143].

$$Specific\ capacity\ (mAh\ g^{-1}) = 1/vW \int_{V_1}^{V_2} iVdV \quad (8)$$

In this equation v is the scan speed in mV/s, W is the weight of the active material, V_1 and V_2 define the potential limits of reduction or oxidation current. Which area of the CV to integrate depends on if the charge or discharge capacity is to be calculated and if the electrode material is used as a positive or negative electrode. The different areas corresponding to charge and discharge capacity is marked in Figure 19. These calculations can be used to evaluate and compare materials to assess the capacity and feasibility for further studies. For more accurate measurements of the capacity, galvanostatic cycling, similar to actual charge and discharge of a cell, should be used.

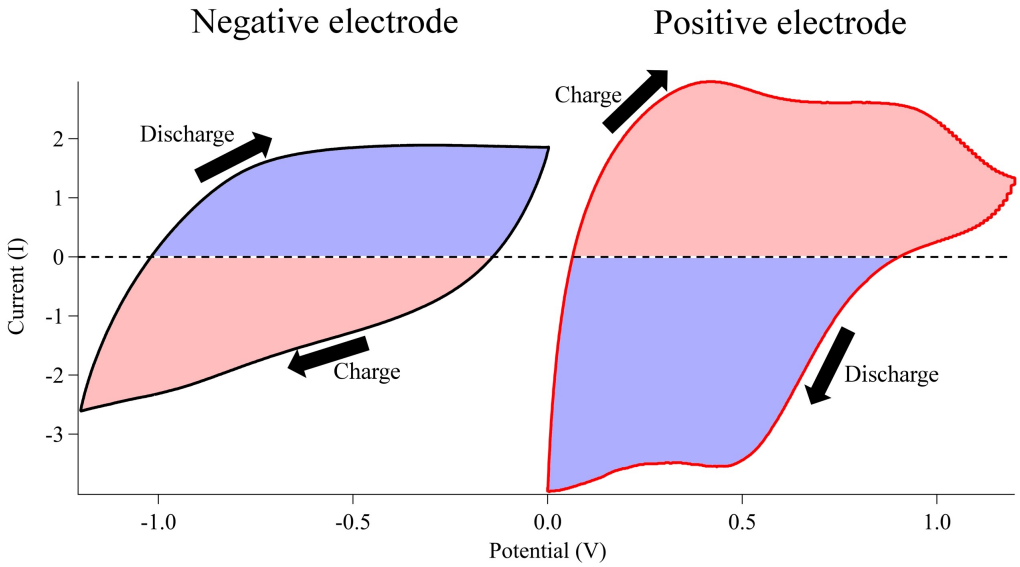

Figure 19. A positive and a negative electrode with respective areas corresponding to charge and discharge capacity in a full cell.

The potential limits of the cycles need to be selected in order to avoid electrochemical decomposition of the electrolyte. If the potential limits are set to wide, the electrolyte will be irreversibly decomposed and to narrow limits might leave out electrochemical reactions. If a new electrolyte is used in an experiment, the upper and lower limits of the electrolyte should first be determined. The simplest method is to cycle the cell with a successively increasing potential window until the current reaches a certain threshold value marking the onset of decomposition. A common criterium is usually around 0.2 mA/cm^2 [144]. Another way to determine the potential limits involve analyzing the efficiency and its derivative with increasing potential windows [145]. The efficiency is calculated taking the second derivative of a so-called S-value which is defined for the positive limit and inversely for the negative limit

$$S_{pos} = \frac{Q_{pos}}{Q_{neg}} - 1 \quad (9)$$

Where Q_{pos} is the charge capacity of the positive electrode and Q_{neg} is the discharge capacity. It is a measure on when side reactions are starting to take place on activated carbon electrodes where the decomposition might be hidden by a double layer current, and it has been proven as an useful method for symmetric supercapacitors [10]. Once the potential window of the system is determined, the limits can be set to arbitrary values. But for practical applications the limits should be set to where the electrode is assumed to operate in a full cell setup.

5.3 Galvanostatic cycling

During galvanostatic cycling, also commonly referred to as constant current cycling (CC), the current in the experiment is kept constant while the voltage response is measured. This results in a figure where the potential is plotted against the time. This way of cycling is similar to how charge storage devices operate. In a potential profile the peaks found in a CV are converted into plateaus whereas a linear slope corresponds to a horizontal line in the CV. Two examples of potential profiles of the same materials as in Figure 16 can be seen in Figure 20.

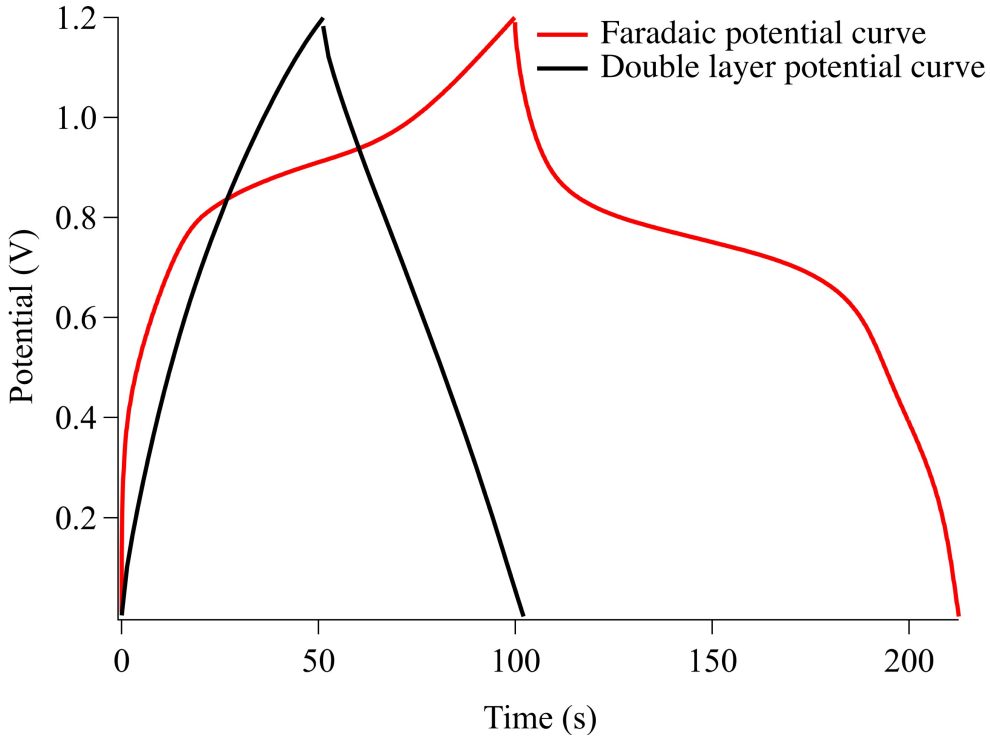

Figure 20. Potential profiles of two materials, TiO_2 with faradaic and activated carbon with double layer charge storage in 0.5 M LiTFSI/EMIM TFSI.

Galvanostatic cycling is a useful tool to calculate and compare the capacity of individual electrodes and the energy and power densities of full cells at different current densities. To calculate the charge or discharge capacity of an electrode the current applied is multiplied with the charge or discharge time of the cycle. From the potential profile it is also possible to assess the electrochemical behavior of a material, or full cell, at different current densities. Such a comparison is illustrated in Figure 21, where the same material is compared at three different current densities. The evolution of the profile is quite typical to this type of measurements. The potential drop at the start of the discharge increases, which follows Ohms law. The profile gradually turns more linear as an effect of a larger contribution from double layer charge storage with increasing current densities. Another important property that is easier to analyze in galvanostatic cycling is the IR-drop, marked in Figure 21. The IR-drop is a measure on how resistive the system is at different current densities.

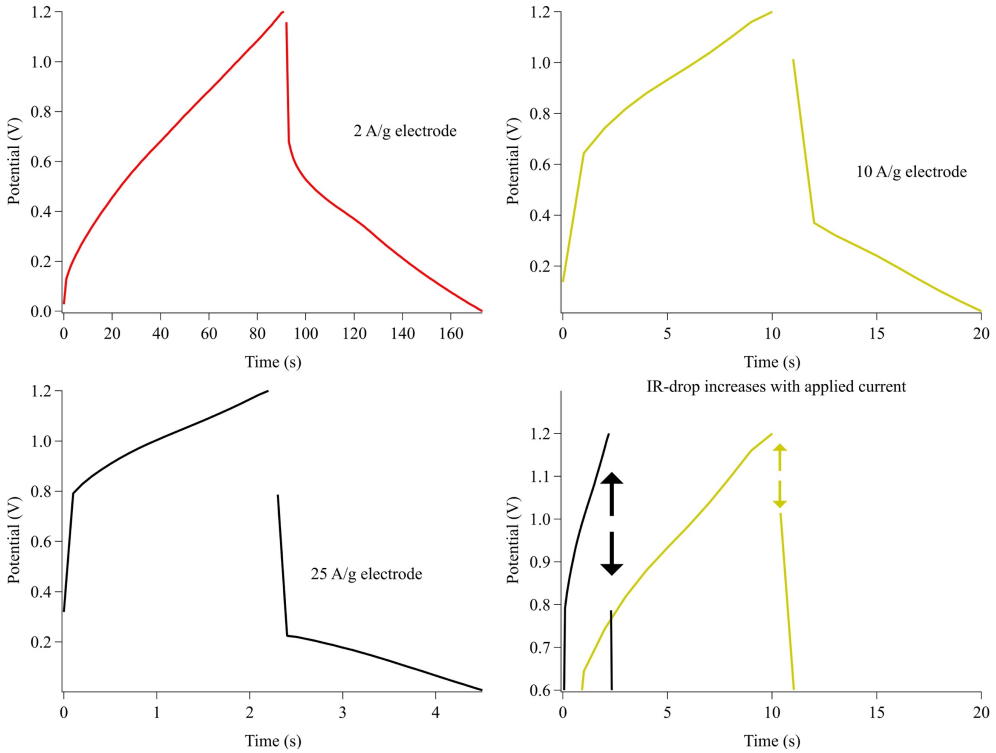

Figure 21. Potential profiles of a VO_2 electrode in 8 m NaTFSI at three different current densities, and the effect on the IR-drop.

Extended galvanostatic cycling is used to evaluate the lifetime of a cell or electrode. The most traditional way of assessing the lifetime is to record the capacity and efficiency as a function of cycle number. This can work for many applications, but in a recent proposed method the potential is kept constant at the maximum or minimum limit for several hours, only doing occasional cycles to measure the charge/discharge capacity [146]. By holding the potential at the limit, it is possible to examine if any parasitic reactions occur that would only have been seen after extremely extensive cycling.

If the energy density of a cell or capacity of an electrode is to be evaluated and it is important to choose a specific current resulting in relevant cycle times for supercapacitor applications. Measuring a high capacity or energy density is not so relevant if the cycle time is the same as that of battery. Supercapacitors are high-power devices and the performance of a device or electrode should be measured and evaluated at high-power conditions [147].

5.4 Electrical impedance spectroscopy

In electric impedance spectroscopy (EIS) an electric pulse with a sinusoidal shape, with the amplitude of typically around 10 mV, used to perturb the electrode and the surrounding electrolyte and the response of the system is recorded. The complex impedance of the system can be represented as [148]

$$Z = \frac{E}{I} = Z_0(\cos(\varphi) + j\sin(\varphi)) \quad (10)$$

where Z_0 is the impedance, E is the potential and I is the current recorded. Further details about the mathematical theory behind this concept is outside the scope of this thesis but can be found in [148]. The imaginary and real parts of the impedance in Eq. 10 represent different properties

of the system. To analyze impedance spectra, so-called Nyquist plots [3,143] are commonly used. In a Nyquist plot the real part is plotted on the x-axis and the imaginary part on the y-axis. An example of a typical impedance response in a Nyquist plot from a composite supercapacitor electrode is shown in Figure 22, the low frequency part is on the right side in the figure and the high-frequency part is to the left. The semi-circle like profile in the high-frequency part is connected with the charge transfer resistance of the electrode, a wider semi-circle corresponds to a more resistive electrode [143].

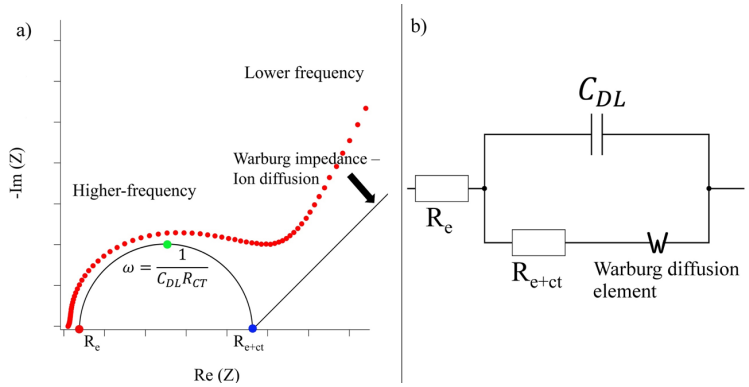

Figure 22a) Impedance spectrum of a cell consisting of a composite MnO_2/CNF electrode and EMIM TFSI ionic liquid electrolyte. Every point represents the response at a single frequency. With higher frequencies to the left. b) The Randles circuit used to model simple diffusion limited reactions at electrode surfaces.

To model the EIS response, electrical circuits are often used. For example, the spectrum in Figure 9a) can approximately be fitted by the circuit in Figure 9b). Where R_e corresponds to the electrolyte resistance, R_{ct} is the charge transfer resistance, C_{DL} is the interphase capacitance and the Warburg resistance, but related to the diffusion of ions to or from the electrode. The resulting curve from this very simple model is shown in Figure 9a [148]. However, this is a very simple model for a complex system, to actually fit the spectra the constants of the Warburg element and the other parts of the circuits are iterated and more components added to the circuit. An interpretation of the spectrum is that at higher frequencies the charge-transfer resistance dominates and then at a certain frequency the ion diffusion will dominate and the spectra will form a straight line. Finding the right equivalent circuit can be difficult and a common problem is that more complicated circuits can be re-arranged in a multitude of different circuits giving exactly the same mode, so how do you know which one is right? [148] The science in fitting spectra with circuits and the interpretation is beyond the scope of this thesis.

EIS can be used to measure any differences in the charge transfer mechanism of the electrode during cycling. Changes in the electrode and the electrode/electrolyte interface will be observed in the semi-circle in the high frequency part of the spectra, this also means that measurement times can be kept relatively short since only the high frequency part is used which is important for in situ measurements of supercapacitors. The type of changes that can be observed are for example the formation of SEI-layers at the surface and changes in morphology at the surface [149].

6. Results

The charge storage mechanism of a supercapacitor depends on the properties of both electrolyte and the electrode material. In **Paper I** this is clearly shown, where two aqueous electrolytes are compared to an ionic liquid. The ionic liquid, with its wider electrochemical stability window, enables a device with higher energy density even though the specific capacities of the electrodes in the aqueous electrolytes are actually higher. However, if both the capacity and the width of the operating voltage window could be improved this would even further increase the energy content of the device.

Below the main results from the different studies on faradaic materials and new electrolytes are presented. In the first part, the results from the investigation of faradaic materials and their interaction with different ionic liquid-based electrolytes are compared and discussed. In the second part, the application of a highly concentrated aqueous electrolyte in combination with a faradaic electrode material is discussed. Finally, in the last part the influence of electrode morphology and its impact on charge storage is investigated and discussed.

6.1 Charge storage mechanisms of faradaic materials with ionic liquid electrolytes

The aim with the studies presented in **Paper II**, **Paper III** and **Paper IV** was to investigate if and how ionic liquids could enable a faradaic contribution from transition metal oxide-based electrodes to the total capacity.

The choice of ionic liquids was motivated by the hypothesis that proton activity or alkali metal cations could enable a faradaic contribution to the total capacity in analogy with proposed mechanisms for aqueous electrolytes [73,74]. To investigate this a aprotic IL was compared to a protic IL and two Brønsted-acid ILs. The different ILs used in these studies are shown in Figure 23.

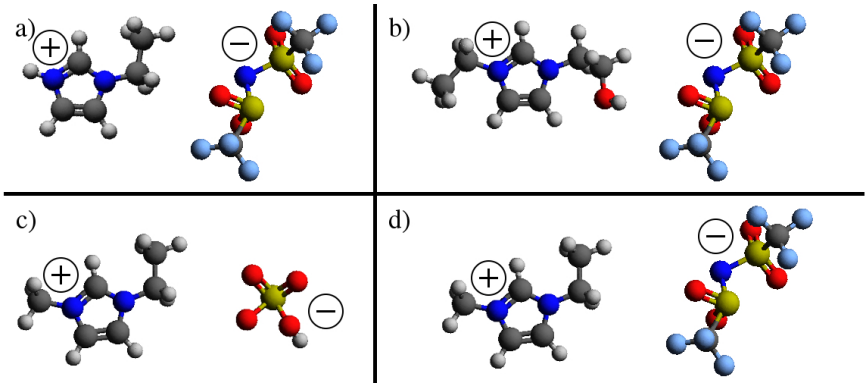

Figure 23. The structure of a) EIM TFSI (protic), b) EtOHIM TFSI (aprotic Brønsted-acid), c) EMIM HSO_4 (aprotic Brønsted-acid) and d) EMIM TFSI (aprotic)

The results of the study on MnO_2 materials showed that the charge storage mechanism strongly depended on the hydrogen-bond forming ability of the IL. In the protic IL a large contribution to the charge storage was obtained from the MnO_2 material. In the aprotic ionic liquids no, or very little, faradaic charge storage was obtained, regardless if hydrogen bonding functional groups are attached or not. Even for the very acidic anion HSO_4, which was by far the strongest proton donor tested in this project, only a small faradaic contribution could be seen. The

structure of the MnO_2 had little effect on the response, indicating predominantly surface based reactions. Expanding the potential window to more negative potentials resulted in poor capacity retention for the protic IL which is explained by MnO_2 dissolution or changes in the surface structure.

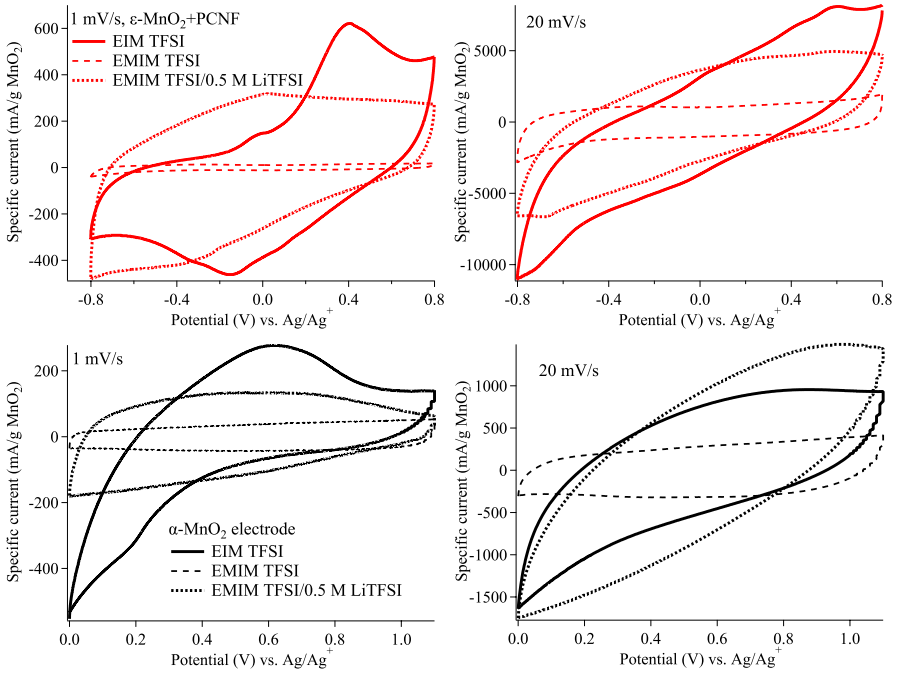

Figure 25. CVs at 1 and 20 mV/s of the ε-MnO_2 and α-MnO_2 electrodes in EMIMTFSI, 0.5M LiTFSI/EMIMTFSI and EIMTFSI. Note that in the upper figures the potential limits are +/- 0.8 V while in the lower it is 0 – +1.1 V.

Figure 25 shows the CVs in the protic, aprotic and LiTFSI doped ILs. A faradaic behavior is obtained with EIMTFSI indicating that the EIM cation interacts with the MnO_2 material. For the neat EMIMTFSI the charge is stored as double layer formation. From ab-initio calculations the interaction energy of the protic EIM cation and the MnO_2 surface was found to be much higher than for the aprotic EMIM ion. And a clear bend in the EIM ion indicate a hydrogen-bond like interaction with the surface, seen in Figure 26. There was also a lack of interaction, both in the experimental and computational results, between the aprotic ILs with hydrogen bonding functional groups attached to one of the ions, which shows that the interaction depends on the strength and position of the available proton.

The experimentally obtained capacity of the α-MnO_2 in EIM TFSI is in good agreement with a perpendicular ordering of the cations at the MnO_2 surface, which was found by calculating the surface coverage and assuming 1 electron/cation. The higher specific current and specific capacity obtained from the CVs in Figure 25 is explained by the lower MnO_2 mass loading and smaller MnO_2 particles in the ε-MnO_2 electrode, further discussed below.

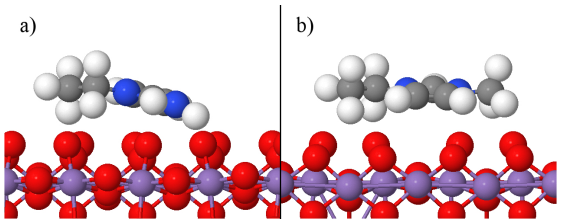

Figure 26. The optimized structures of a) EIM and b) EMIM cations at an MnO_2 surface.

The results above are in good agreement with previous results for thin MnO_2 electrodes in protic ILs [78]. It contradicts previous results claiming MnO_2 interaction with neat aprotic ILs [76,77]. Standing cations contradicts previous findings showing a parallel configuration of ions [61]. The capacity fade observed when MnO_2 is cycled at a lower potential is in line with previous results in aqueous electrolytes where in situ measurements attributed it to MnO_2 dissolution and irreversible phase changes to less active species [72].

In the 0.5 M LiTFSI/EMIMTFSI electrolyte the faradaic contribution results in broader peaks due to a difference in surface layer composition and ion diffusion in the electrolyte. Hence in the 0.5M LiTFSI/EMIMTFSI electrolyte only the Li-ion interacts with the MnO_2 and the slower diffusion of Li-ions through surface layers of EMIM ions explains the broader peaks. The Li-ion interaction with the surface was further investigated by comparing the MnO_2 material with TiO_2.

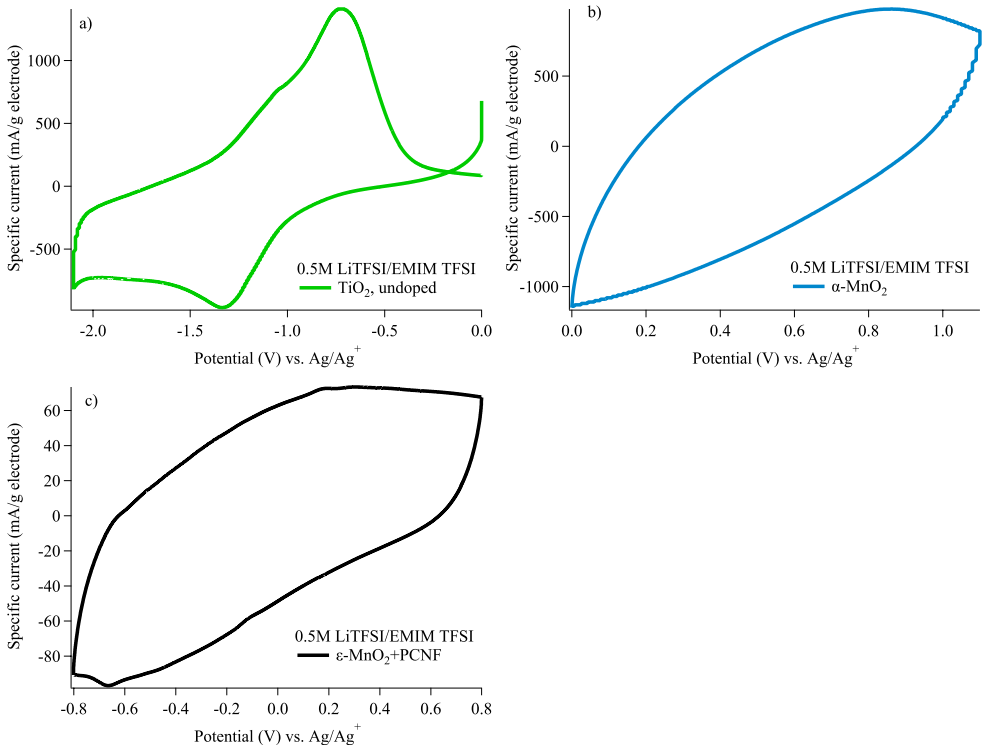

Figure 28. CVs of a) TiO_2, b) α-MnO_2 and c) ε-MnO_2/CNF at 10 mV/s in 0.5 M LiTFSI/EMIM TFSI.

The peaks of the CVs in Figure 28 show the dominating insertion-type charge storage mechanism in TiO_2 with clear peaks visible. The sharper peaks for TiO_2 is explained by a much more facile insertion of Li-ions into the structure. Not only the Li-ions moves easier in the TiO_2 material, the higher electrical conductivity of TiO_2 explains the more tilted CVs of the MnO_2 materials compared to TiO_2. Even for the MnO_2 composite material. The broadening of the

peak of TiO_2 in an ionic liquid electrolyte could indicate that a screening effect of the EMIM ions occurs in this system as well.

These results are in good agreement with previous results that has shown that Li-insertion only occurs in ε-MnO_2 at significantly lower potentials [150], while Li-insertion occurs in α-MnO_2 the lithium diffusion coefficient is about two orders of magnitude lower [151] than in TiO_2 [89]. The shape of the TiO_2 is in good agreement with previous results using IL electrolytes [152].

6.2 Interaction of highly-concentrated electrolytes and hybrid electrodes

The aim with **Paper VI** was to investigate how the charge storage mechanism of a metal oxide is affected by the transition from a strongly alkaline electrolyte to a HCE, and how the high scan rate performance is compared to other systems using ILs and organic solvents as electrolytes.

The HCE enabled an increased potential window, from 0.5 V in the alkaline electrolyte to 1.2 V in the HCE and as a result, the capacity of the VO_2 increased as well. In Figure 29 the CVs of VO_2 alkaline 6 M KOH and neutral 8 m NaTFSI is compared at 10 and 100 mV/s. The broad peak during oxidation and reduction is attributed to two redox-reactions occurring. In the KOH electrolyte the narrower peak and reduced peak separation is attributed to the higher conductivity of the electrolyte. The increased capacity can be explained by the suggested reactions in Eq. 11.

$$V(IV)O_2 + aNa^+ + ae^- \leftrightarrow Na_xV(IV\text{-}a)O_2 \quad (11)$$

where the Na^+ is the cation in the electrolyte, the initial oxidation state of the vanadium atom is assumed to be V^{+4} X is the number of electrons taking place in the reactions. The higher capacity of VO_2 in the 8 m NaTFSI electrolyte is explained by additional oxidation state becoming available in the expanded potential window contributing with more electrons in Eq. 11.

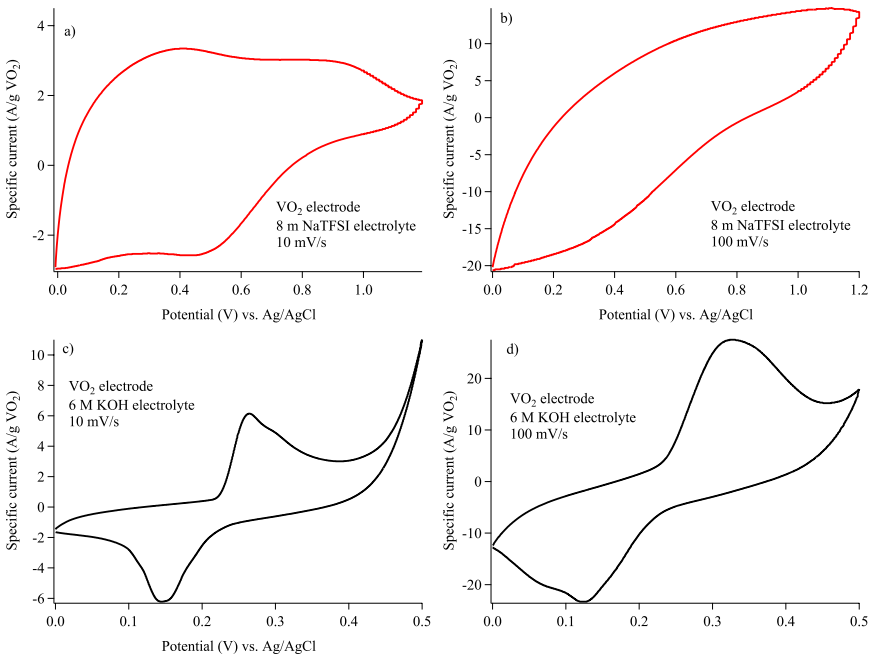

Figure 29. Comparing CVs of a VO_2 electrode in 8 m NaTFSI (top) at a) 10 mV/s and b) 100 mV/s and 6 M KOH at a) 10 mV/s and b) 100 mV/s.

The cycle lifetime was however not improved, the capacity decreased over just a couple of hundred cycles. The poor capacity retention in Figure 30 compared to the KOH electrolyte [153] can also be explained by the additional redox-reaction taking place when oxidized to 1.2 V, which causes dissolution or structural changes of the material surface in a similar way as ε-MnO_2 at lower potentials or due to electrolyte decomposition.

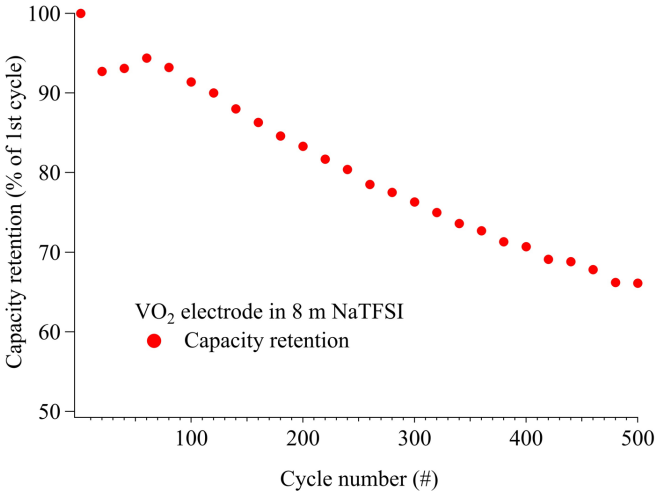

Figure 30. The capacity retention of the VO_2 electrode cycled in 8 m NaTFSI.

The relative voltammetric capacity of the system was compared with that of TiO_2/LP30 and TiO_2/0.5 M LiTFSI/EMIMTFSI systems despite the higher conductivity of the HCE, a lower relative capacity was obtained, Figure 31. The relative voltammetric charge is higher in the TiO_2/LP30 system at all scan speed, despite having approximately the same conductivity as 0.5 M LiTFSI/EMIMTFSI and considerably lower than the 8 m NaTFSI electrolyte. This behaviour is explained by an easier Li-insertion in the LP30 electrolyte compared to the IL, where the EMIM ions block the surface from the Li-ions together with a lower viscosity of the IL. At even

faster scan speeds the double layer contribution dominates the charge storage at which point the high electrical conductivity of the TiO_2 and slightly larger surface area is beneficial.

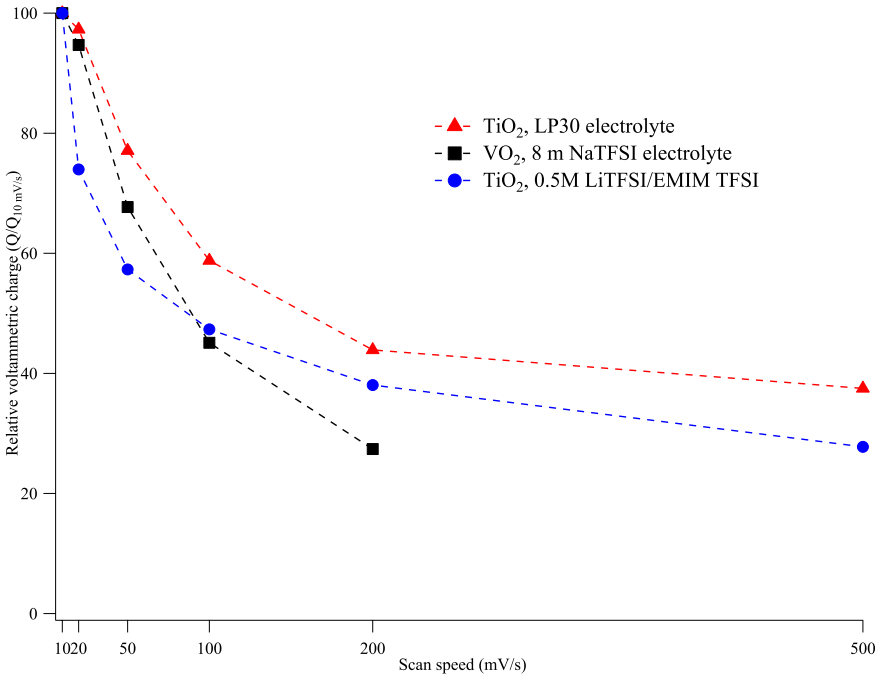

Figure 31. Relative voltammetric discharge of VO_2 in 8 m NaTFSI and TiO_2 in LP30 and 0.5 M LiTFSI/EMIMTFSI at various scan speeds.

The results presented on the HCE/VO_2 system above are in good agreement with previous results on VO_2(B) materials, with no improvement in cycle stability and with a slightly lower capacity [41] explained by the relatively low surface area of the VO_2 material, reducing the contribution from surface-active redox reactions. The comparison between the relative voltammetric charge show the importance of ensuring both a highly conducting electrode and electrolyte.

6.3 The effect of material morphology and structure and the interaction with organic solvent and ionic liquid electrolytes

In **Paper II**, **III**, **IV**, **V** and **VI** the effect of the morphologies and structures of the electrodes on the charge storage mechanism is also investigated. Showing the importance of nanoscaling the particles to reduce unused volume and improve the capacity at high scan speeds.

In Figure 32 are SEM images of four different morphologies and three different materials. Figure 32a shows the TiO_2 particles with the microbead morphology consisting of nanocrystallites. It has an excellent cycle stability and provides high capacity even at a low specific surface of 90 m^2/g due to facile Li-insertion. Changing the VO_2 morphology from b to c increases capacity significantly but only increases the surface area slightly, so the additional capacity is explained by a slight change in the lattice parameter for the material in Figure 34c. Figure 34d is of the MnO_2/CNF composite showing an individual carbon fiber coated with a thin layer of MnO_2 with a hair-like texture.

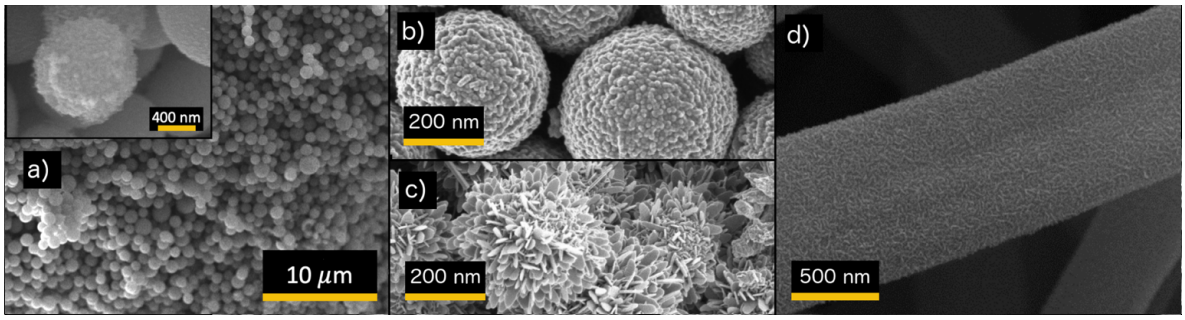

Figure 32. SEM images of a) TiO_2 anatase microbeads, b-c) VO_2(B) and d) MnO_2/composite.

The improvement of changing from an electrode consisting of relatively large MnO_2 particles to an electrode consisting of nanosized particles evenly distributed on a conductive substrate is illustrated in Figure 33. The increased relative voltammetric charge is dramatically improved in both electrolytes. However, using substrates with even higher surface area would be more beneficial to further increase capacity of the electrode.

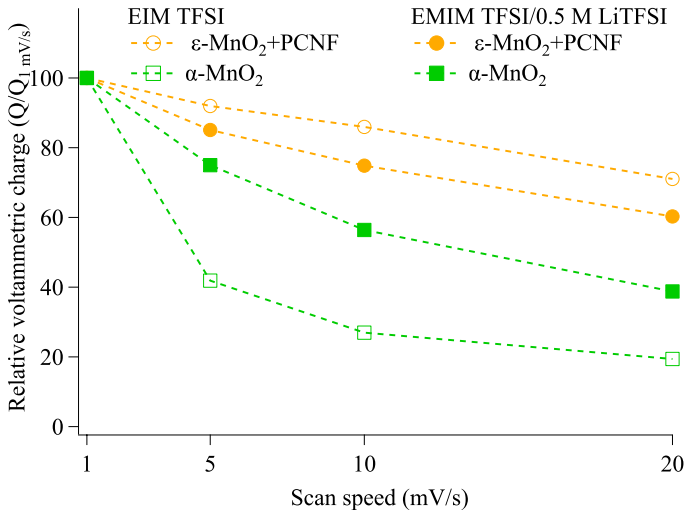

Figure 33. The relative charge at different scan speeds for α-MnO_2 and ε-MnO_2/CNF in EIM TFSI and 0.5M LiTFSI/EMIM TFSI.

The change in atomic structure was discussed for VO_2 above, but was also considered for TiO_2. Doping the TiO_2 microbeads improved the electronic conductivity of the material, without affecting the nanocrystalline structure of the microbeads. The unique structure and morphology of the TiO_2 microbead induce an irreversible structure change of the surface in an ionic liquid electrolyte. Seen in Figure 32.

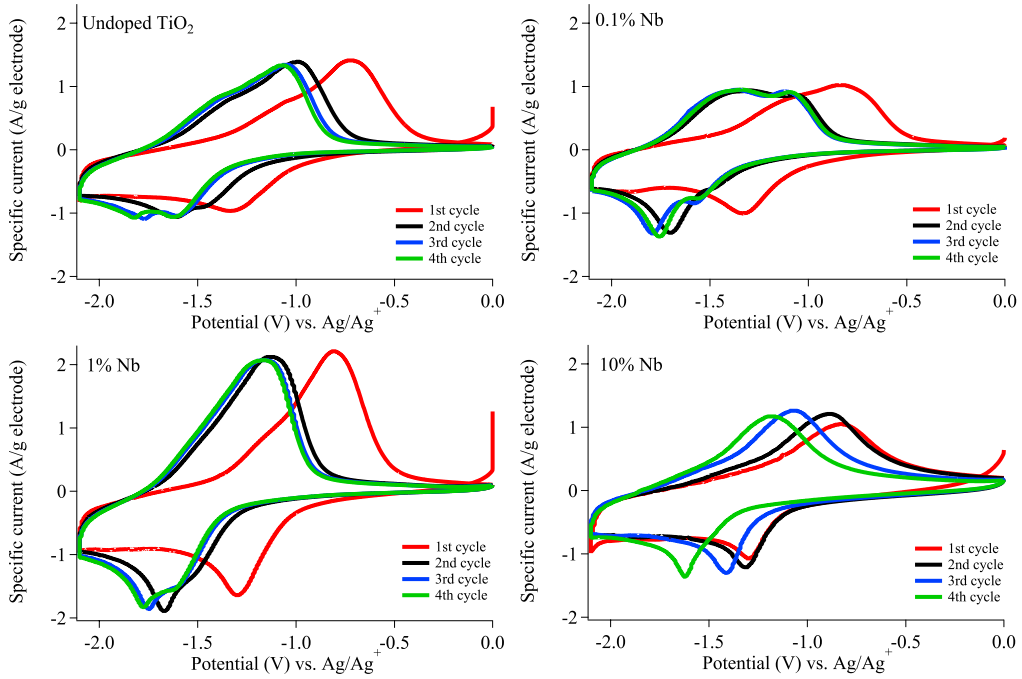

Figure 34. Comparison of the four first cycles of the different TiO_2 materials at 10 mV/s in 0.5M LiTFSI/EMIM TFSI.

The changes in shape of the CVs in the first cycle of the TiO_2 material doped with Nb is attributed to the increased electrical conductivity. In the second to fourth cycle the shape of the CVs changes, which is attributed to a lowered conductivity of electrode as a result of the formation of new phases in the electrode. The structural change is unfortunately detrimental to the high-power density. However, as seen in Figure 35, it has a positive effect on the cycle lifetime, preventing the initial capacity fade seen when using the LP30 which is a common feature of TiO_2 in most other systems.

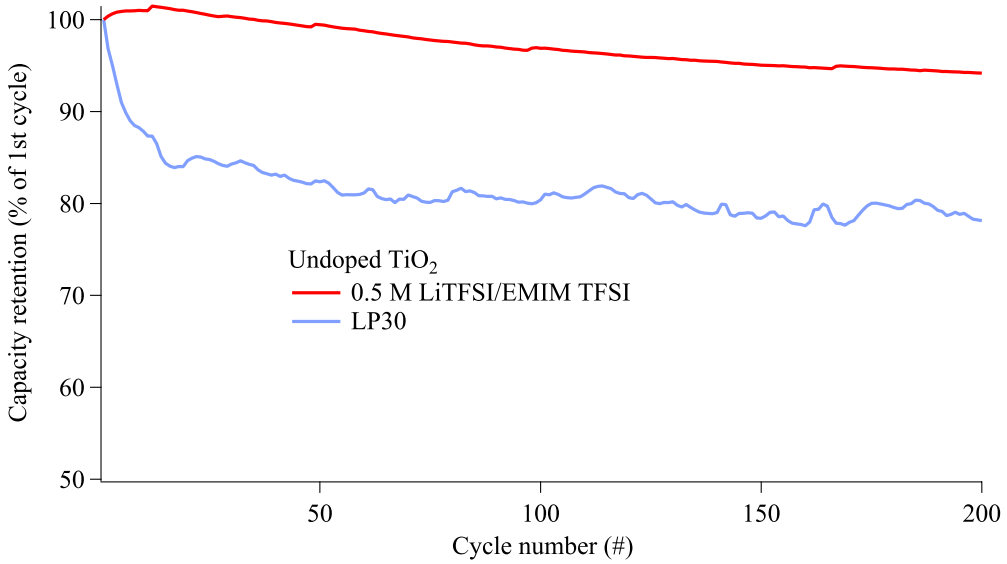

Figure 35. Cycle lifetime of undoped TiO_2 cycled in 0.5 M LiTFSI/EMIM TFSI and LP30.

7. Outlook

Considering the future research in this field, determining the oxidation number and change of the MnO_2 electrode in the protic IL would be of great interest to be able to compare the redox reaction with conventional electrolytes. Further expansion of the research with more systems of faradaic materials and other protic ILs, both negative and positive electrodes would be a systematic study that could provide valuable understanding.

To design a full cell with IL induced redox reactions as the faradaic contribution would also be interesting. It could also be tempting to try to design a cell with no metal parts, using self-standing electrodes of conductive polymers and ionic liquid based electrolytes. High-temperature operation for IL based systems is also interesting, especially with VO_2 due to its low-temperature transition from insulator to metal at 80 °C which could enable a high conductivity of the electrode and electrolyte. Regarding the TiO_2 material, investigating if the stabilization process in the IL could be transferred to an organic electrolyte could be interesting. Is it possible to avoid the initial capacity fade by first cycling the electrode in an ionic liquid electrolyte?

8. Acknowledgement

First of all, I would like to thank my ‘Tenzig Norgay’, my supervisor, Professor Aleksandar Matic who helped my climb this mountain of a thesis and who has taught me one or two things along the way. Thank you for the good scientific discussions, the freedom in my research and letting me visit conferences and really growing during these five years!

Next in line is of course Professor Patrik Johansson who once employed me five years ago, for letting me be a part of the PJ ‘solar system’ and the scientific discussions and advice! But also, for sending me to South Africa, thank you for that experience!

I would also like to thank Ezio for helping out with measurements and fixing things that (other people) have messed up in the lab…

Since I’ve already been mentioned in one acknowledgement I want to thank Gustav for enduring these five years in the same office! What adventures we have been on, dodgy taxi rides in South Africa, road tripping in Japan, arguments on the best TV-shows mixed with some sound scientific discussion every now and then. It has been a very good time so far!

I would also like to thank all members of (K)MF, present and former, that really have made this a fantastic time! You guys are awesome, and I’m really going to miss this place!

I would like to thank all the people down at UP, Professor Ncholu Manyala for welcoming me, providing for excellent scientific results through a very nice collaboration. It was a fantastic experience! I would also like to thank all the other people that I have collaborated with during the years, Professors Thierry Brousse and Jean Le Bideau at the University of Nantes for providing with good discussions regarding Paper I, it was very helpful!

I want to thank the Swedish Energy Agency for the funding through ‘Batterifonden #39042-1’

Finally, last, but not least I would like to thank my family for supporting me during these years, I could not have done it without you! Tack!

References

[1] M.M. Kabir, D.E. Demirocak, Degradation mechanisms in Li-ion batteries: a state-of-the-art review, Int. J. Energy Res. 41 (2017) 1963–1986. https://doi.org/10.1002/er.3762.

[2] C. Schütter, S. Pohlmann, A. Balducci, Industrial Requirements of Materials for Electrical Double Layer Capacitors: Impact on Current and Future Applications, Adv. Energy Mater. 9 (2019) 1900334. https://doi.org/10.1002/aenm.201900334.

[3] F. Beguin, E. Frackowiak, eds., Supercapacitors : Materials, Systems and Applications, John Wiley & Sons, 2013.

[4] S.W. Lee, J. Kim, S. Chen, P.T. Hammond, Y. Shao-Horn, Carbon Nanotube/Manganese Oxide Ultrathin Film Electrodes for Electrochemical Capacitors, ACS Nano. 4 (2010) 3889–3896. https://doi.org/10.1021/nn100681d.

[5] R.B. Rakhi, D.H. Nagaraju, P. Beaujuge, H.N. Alshareef, Supercapacitors based on two dimensional VO2nanosheet electrodes in organic gel electrolyte, Electrochim. Acta. 220 (2016) 601–608. https://doi.org/10.1016/j.electacta.2016.10.109.

[6] W. Sugimoto, T. Kizaki, K. Yokoshima, Y. Murakami, Y. Takasu, Evaluation of the pseudocapacitance in RuO_2 with a RuO_2/GC thin film electrode, Electrochim. Acta. 49 (2004) 313–320. https://doi.org/10.1016/j.electacta.2003.08.013.

[7] V. Augustyn, P. Simon, B. Dunn, Pseudocapacitive oxide materials for high-rate electrochemical energy storage, Energy Environ. Sci. 7 (2014) 1597. https://doi.org/10.1039/c3ee44164d.

[8] C. Zhong, Y. Deng, W. Hu, J. Qiao, L. Zhang, J. Zhang, A review of electrolyte materials and compositions for electrochemical supercapacitors, Chem. Soc. Rev. 44 (2015) 7484–7539. https://doi.org/10.1039/C5CS00303B.

[9] A. Brandt, P. Isken, A. Lex-Balducci, A. Balducci, Adiponitrile-based electrochemical double layer capacitor, J. Power Sources. 204 (2012) 213–219. https://doi.org/10.1016/j.jpowsour.2011.12.025.

[10] D. Reber, R.-S. Kühnel, C. Battaglia, High-voltage aqueous supercapacitors based on NaTFSI, Sustain. Energy Fuels. (2017). https://doi.org/10.1039/C7SE00423K.

[11] C. Arbizzani, M. Biso, D. Cericola, M. Lazzari, F. Soavi, M. Mastragostino, Safe, high-energy supercapacitors based on solvent-free ionic liquid electrolytes, J. Power Sources. 185 (2008) 1575–1579. https://doi.org/10.1016/j.jpowsour.2008.09.016.

[12] A. Muzaffar, M.B. Ahamed, K. Deshmukh, J. Thirumalai, A review on recent advances in hybrid supercapacitors: Design, fabrication and applications, Renew. Sustain. Energy Rev. 101 (2019) 123–145. https://doi.org/10.1016/j.rser.2018.10.026.

[13] H.I. Becker, Low voltage electrolytic capacitor, US2800616A, 1954.

[14] A.K. Samantara, S. Ratha, Historical Background and Present Status of the Supercapacitors, in: Mater. Dev. Act. Components a Supercapacitor Background, Present Status Futur. Perspect., Springer Singapore, Singapore, 2018: pp. 9–10. https://doi.org/10.1007/978-981-10-7263-5_2.

[15] X. Feng, Nanocarbons for Advanced Energy Conversion, Wiley, Newark, UNITED STATES, 2015. http://ebookcentral.proquest.com/lib/chalmers/detail.action?docID=2075769.

[16] TOSA: A new generation of buses, (n.d.). https://new.abb.com/grid/technology/tosa (accessed April 9, 2020).

[17] Opening doors to space, (n.d.). https://www.esa.int/Applications/Telecommunications_Integrated_Applications/Opening_doors_to_space (accessed April 9, 2020).

[18] Scott Patrol e-1 Avalanche Backpack, (n.d.). https://www.scott-

sports.com/global/en/page/patrol-e1-avalanche-backpack (accessed April 9, 2020).
[19] NTU and BlueSG launch ultra-fast charging electric shuttle, (n.d.). http://media.ntu.edu.sg/NewsReleases/Pages/newsdetail.aspx?news=f80a11bf-0702-455a-8f57-a80bcf18db3a (accessed April 8, 2020).
[20] S.C. Lee, W.Y. Jung, Analogical understanding of the Ragone plot and a new categorization of energy devices, Energy Procedia. 88 (2016) 526–530. https://doi.org/10.1016/j.egypro.2016.06.073.
[21] D.P. Dubal, O. Ayyad, V. Ruiz, P. Gomez-Romero, Hybrid energy storage: the merging of battery and supercapacitor chemistries, Chem. Soc. Rev. 44 (2015) 1777–1790. https://doi.org/10.1039/C4CS00266K.
[22] Maxwell Technologies, (n.d.). https://www.maxwell.com/products/ultracapacitors (accessed April 8, 2020).
[23] Skeleton Technologies, (n.d.). https://www.skeletontech.com/skelmod-170v-ultracapacitor-module (accessed April 8, 2020).
[24] AEP International, (n.d.). https://www.aepint.nl/hybrid-power/products/ultracapacitors-modules/ (accessed April 8, 2020).
[25] B.E. Conway, Transition from "Supercapacitor" to "Battery" Behavior in Electrochemical Energy Storage, J. Electrochem. Soc. 138 (1991) 1539. https://doi.org/10.1149/1.2085829.
[26] F. Béguin, V. Presser, A. Balducci, E. Frackowiak, Carbons and electrolytes for advanced supercapacitors, Adv. Mater. 26 (2014) 2219–2251. https://doi.org/10.1002/adma.201304137.
[27] L. Suo, O. Borodin, T. Gao, M. Olguin, J. Ho, X. Fan, C. Luo, C. Wang, K. Xu, "Water-in-salt" electrolyte enables high-voltage aqueous lithium-ion chemistries, Science (80-.). 350 (2015). https://doi.org/10.1126/science.aab1595.
[28] K. Nomura, H. Nishihara, N. Kobayashi, T. Asada, T. Kyotani, 4.4 V Supercapacitors Based on Super-Stable Mesoporous Carbon Sheet Made of Edge-Free Graphene Walls, Energy Environ. Sci. 12 (2019) 1542–1549. https://doi.org/10.1039/c8ee03184c.
[29] H. Lu, X.S. Zhao, Biomass-derived carbon electrode materials for supercapacitors, Sustain. Energy Fuels. 1 (2017) 1265–1281. https://doi.org/10.1039/C7SE00099E.
[30] S. Trasatti, G. Buzzanca, Ruthenium dioxide: a new interesting electrode material. Solid state structure and electrochemical behaviour, Electroanal. Chem. Interfacial Electrochistry. 29 (1971) 1689–1699. https://doi.org/10.1017/CBO9781107415324.004.
[31] B.E. Conway, Electrochemical Supercapacitors, 1999. https://doi.org/10.1007/978-1-4757-3058-6.
[32] Q. Meng, K. Cai, Y. Chen, L. Chen, Research progress on conducting polymer based supercapacitor electrode materials, Nano Energy. 36 (2017) 268–285. https://doi.org/10.1016/j.nanoen.2017.04.040.
[33] M. Cakici, K.R. Reddy, F. Alonso-Marroquin, Advanced electrochemical energy storage supercapacitors based on the flexible carbon fiber fabric-coated with uniform coral-like MnO2structured electrodes, Chem. Eng. J. 309 (2017) 151–158. https://doi.org/10.1016/j.cej.2016.10.012.
[34] S. Cho, J. Kim, Y. Jo, A.T.A. Ahmed, H.S. Chavan, H. Woo, A.I. Inamdar, J.L. Gunjakar, S.M. Pawar, Y. Park, H. Kim, H. Im, Bendable RuO_2/graphene thin film for fully flexible supercapacitor electrodes with superior stability, J. Alloys Compd. 725 (2017) 108–114. https://doi.org/10.1016/j.jallcom.2017.07.135.
[35] N. Arun, A. Jain, V. Aravindan, S. Jayaraman, W. Chui Ling, M.P. Srinivasan, S. Madhavi, Nanostructured spinel $LiNi_{0.5}Mn_{1.5}O_4$ as new insertion anode for advanced Li-ion capacitors with high power capability, Nano Energy. 12 (2015) 69–75.

https://doi.org/10.1016/j.nanoen.2014.12.006.
[36] L. Ye, Q. Liang, Y. Lei, X. Yu, C. Han, W. Shen, Z.H. Huang, F. Kang, Q.H. Yang, A high performance Li-ion capacitor constructed with $Li_4Ti_5O_{12}$/C hybrid and porous graphene macroform, J. Power Sources. 282 (2015) 174–178. https://doi.org/10.1016/j.jpowsour.2015.02.028.
[37] A. Chaturvedi, P. Hu, V. Aravindan, C. Kloc, S. Madhavi, Unveiling two-dimensional TiS_2 as an insertion host for the construction of high energy Li-ion capacitors, J. Mater. Chem. A. 5 (2017) 9177–9181. https://doi.org/10.1039/c7ta01594a.
[38] D. Ruan, M.S. Kim, B. Yang, J. Qin, K.B. Kim, S.H. Lee, Q. Liu, L. Tan, Z. Qiao, 700 F hybrid capacitors cells composed of activated carbon and $Li_4Ti_5O_{12}$ microspheres with ultra-long cycle life, J. Power Sources. 366 (2017) 200–206. https://doi.org/10.1016/j.jpowsour.2017.09.029.
[39] B.K. Lesel, J.B. Cook, Y. Yan, T.C. Lin, S.H. Tolbert, Using Nanoscale Domain Size to Control Charge Storage Kinetics in Pseudocapacitive Nanoporous $LiMn_2O_4$ Powders, ACS Energy Lett. 2 (2017) 2293–2298. https://doi.org/10.1021/acsenergylett.7b00634.
[40] D. Zhou, H. Lin, F. Zhang, H. Niu, L. Cui, Q. Wang, F. Qu, Freestanding MnO2 nanoflakes/porous carbon nanofibers for high-performance flexible supercapacitor electrodes, Electrochim. Acta. 161 (2015) 427–435. https://doi.org/10.1016/j.electacta.2015.02.085.
[41] Y. Zhang, J. Zheng, T. Hu, F. Tian, C. Meng, Synthesis and supercapacitor electrode of VO_2(B)/C core-shell composites with a pseudocapacitance in aqueous solution, Appl. Surf. Sci. 371 (2016) 189–195. https://doi.org/10.1016/j.apsusc.2016.02.199.
[42] R.R. Bi, X.L. Wu, F.F. Cao, L.Y. Jiang, Y.G. Guo, L.J. Wan, Highly dispersed RuO_2 nanoparticles on carbon nanotubes: Facile synthesis and enhanced supercapacitance performance, J. Phys. Chem. C. 114 (2010) 2448–2451. https://doi.org/10.1021/jp9116563.
[43] Z. Ma, G. Shao, Y. Fan, G. Wang, J. Song, D. Shen, Construction of Hierarchical α-MnO2 Nanowires@Ultrathin δ-MnO_2 Nanosheets Core-Shell Nanostructure with Excellent Cycling Stability for High-Power Asymmetric Supercapacitor Electrodes, ACS Appl. Mater. Interfaces. 8 (2016) 9050–9058. https://doi.org/10.1021/acsami.5b11300.
[44] Q. Qu, P. Zhang, B. Wang, Y. Chen, S. Tian, Y. Wu, R. Holze, Electrochemical performance of MnO_2 nanorods in neutral aqueous electrolytes as a cathode for asymmetric supercapacitors, J. Phys. Chem. C. 113 (2009) 14020–14027. https://doi.org/10.1021/jp8113094.
[45] A.S. Levitt, M. Alhabeb, C.B. Hatter, A. Sarycheva, G. Dion, Y. Gogotsi, Electrospun MXene/carbon nanofibers as supercapacitor electrodes, J. Mater. Chem. A. 7 (2019) 269–277. https://doi.org/10.1039/c8ta09810g.
[46] P. Pazhamalai, K. Krishnamoorthy, V.K. Mariappan, S.J. Kim, Blue TiO_2 nanosheets as a high-performance electrode material for supercapacitors, J. Colloid Interface Sci. 536 (2019) 62–70. https://doi.org/10.1016/j.jcis.2018.10.031.
[47] C. Zhan, W. Liu, M. Hu, Q. Liang, X. Yu, Y. Shen, R. Lv, F. Kang, Z.H. Huang, High-performance sodium-ion hybrid capacitors based on an interlayer-expanded MoS_2/rGO composite: surpassing the performance of lithium-ion capacitors in a uniform system, NPG Asia Mater. 10 (2018) 775–787. https://doi.org/10.1038/s41427-018-0073-y.
[48] J. Yan, C.E. Ren, K. Maleski, C.B. Hatter, B. Anasori, P. Urbankowski, A. Sarycheva, Y. Gogotsi, Flexible MXene/Graphene Films for Ultrafast Supercapacitors with Outstanding Volumetric Capacitance, Adv. Funct. Mater. 27 (2017) 1–10. https://doi.org/10.1002/adfm.201701264.

[49] H. Wang, Y. Liang, T. Mirfakhrai, Z. Chen, H.S. Casalongue, H. Dai, Advanced asymmetrical supercapacitors based on graphene hybrid materials, Nano Res. 4 (2011) 729–736. https://doi.org/10.1007/s12274-011-0129-6.
[50] P. Kubiak, M. Pfanzelt, J. Geserick, U. Hörmann, N. Hüsing, U. Kaiser, M. Wohlfahrt-Mehrens, Electrochemical evaluation of rutile TiO_2 nanoparticles as negative electrode for Li-ion batteries, J. Power Sources. 194 (2009) 1099–1104. https://doi.org/10.1016/J.JPOWSOUR.2009.06.021.
[51] H. Kim, M.Y. Cho, M.H. Kim, K.Y. Park, H. Gwon, Y. Lee, K.C. Roh, K. Kang, A novel high-energy hybrid supercapacitor with an anatase TiO_2-reduced graphene oxide anode and an activated carbon cathode, Adv. Energy Mater. 3 (2013) 1500–1506. https://doi.org/10.1002/aenm.201300467.
[52] Y. Cai, H.E. Wang, S.Z. Huang, M.F. Yuen, H.H. Cai, C. Wang, Y. Yu, Y. Li, W.J. Zhang, B.L. Su, Porous TiO_2 urchins for high performance Li-ion battery electrode: Facile synthesis, characterization and structural evolution, Electrochim. Acta. 210 (2016) 206–214. https://doi.org/10.1016/j.electacta.2016.05.140.
[53] U. Lafont, D. Carta, G. Mountjoy, A. V. Chadwick, E.M. Kelder, In situ structural changes upon electrochemical lithium insertion in nanosized anatase TiO_2, J. Phys. Chem. C. 114 (2010) 1372–1378. https://doi.org/10.1021/jp908786t.
[54] S. Brutti, V. Gentili, H. Menard, B. Scrosati, P.G. Bruce, TiO_2-(B) nanotubes as anodes for lithium batteries: Origin and mitigation of irreversible capacity, Adv. Energy Mater. 2 (2012) 322–327. https://doi.org/10.1002/aenm.201100492.
[55] T. Song, U. Paik, TiO_2 as an active or supplemental material for lithium batteries, J. Mater. Chem. A. 4 (2015) 14–31. https://doi.org/10.1039/c5ta06888f.
[56] B. Gorska, E. Frackowiak, F. Beguin, Redox active electrolytes in carbon/carbon electrochemical capacitors, Curr. Opin. Electrochem. 9 (2018) 95–105. https://doi.org/10.1016/j.coelec.2018.05.006.
[57] D. Pletcher, A First Course in Electrode Processes, The Royal Society of Chemistry, 2009.
[58] A. González, E. Goikolea, J.A. Barrena, R. Mysyk, Review on supercapacitors: Technologies and materials, Renew. Sustain. Energy Rev. 58 (2016) 1189–1206. https://doi.org/10.1016/j.rser.2015.12.249.
[59] Y.Z. Su, Y.C. Fu, Y.M. Wei, J.W. Yan, B.W. Mao, The electrode/ionic liquid interface: Electric double layer and metal electrodeposition, ChemPhysChem. 11 (2010) 2764–2778. https://doi.org/10.1002/cphc.201000278.
[60] M.Z. Bazant, B.D. Storey, A.A. Kornyshev, Double layer in ionic liquids: Overscreening versus crowding, Phys. Rev. Lett. 106 (2011) 6–9. https://doi.org/10.1103/PhysRevLett.106.046102.
[61] A. Elbourne, S. McDonald, K. Voïchovsky, F. Endres, G.G. Warr, R. Atkin, Nanostructure of the Ionic Liquid-Graphite Stern Layer, ACS Nano. 9 (2015) 7608–7620. https://doi.org/10.1021/acsnano.5b02921.
[62] S.S.D. Begić, F. Chen, E. Jónsson, M. Forsyth, Overscreening and crowding in electrochemical ionic liquid systems, Phys. Rev. Mater. 3 (2019) 1–8. https://doi.org/10.1103/PhysRevMaterials.3.095801.
[63] M. McEldrew, Z.A.H. Goodwin, A.A. Kornyshev, M.Z. Bazant, Theory of the Double Layer in Water-in-Salt Electrolytes, J. Phys. Chem. Lett. 9 (2018) 5840–5846. https://doi.org/10.1021/acs.jpclett.8b02543.
[64] M. Oschatz, S. Boukhalfa, W. Nickel, J.P. Hofmann, C. Fischer, G. Yushin, S. Kaskel, Carbide-derived carbon aerogels with tunable pore structure as versatile electrode material in high power supercapacitors, Carbon N. Y. 113 (2017) 283–291. https://doi.org/10.1016/j.carbon.2016.11.050.

[65] L. Negre, B. Daffos, V. Turq, P.L. Taberna, P. Simon, Ionogel-based solid-state supercapacitor operating over a wide range of temperature, Electrochim. Acta. 206 (2016) 490–495. https://doi.org/10.1016/j.electacta.2016.02.013.
[66] N. Jäckel, P. Simon, Y. Gogotsi, V. Presser, Increase in Capacitance by Subnanometer Pores in Carbon, ACS Energy Lett. 1 (2016) 1262–1265. https://doi.org/10.1021/acsenergylett.6b00516.
[67] J. Chmiola, G. Yushin, R. Dash, Y. Gogotsi, Effect of pore size and surface area of carbide derived carbons on specific capacitance, J. Power Sources. 158 (2006) 765–772. https://doi.org/10.1016/j.jpowsour.2005.09.008.
[68] L. Sun, C. Tian, M. Li, X. Meng, L. Wang, R. Wang, J. Yin, H. Fu, From coconut shell to porous graphene-like nanosheets for high-power supercapacitors, J. Mater. Chem. A. 1 (2013) 6462–6470. https://doi.org/10.1039/c3ta10897j.
[69] J. Hou, C. Cao, X. Ma, F. Idrees, B. Xu, X. Hao, W. Lin, From rice bran to high energy density supercapacitors: A new route to control porous structure of 3D carbon, Sci. Rep. 4 (2014) 1–6. https://doi.org/10.1038/srep07260.
[70] B.E. Conway, Electrochemical Supercapacitors, Scientific Fundamentals and Technological Applications, 1999. https://doi.org/10.1017/CBO9781107415324.004.
[71] G.A. Snook, P. Kao, A.S. Best, Conducting-polymer-based supercapacitor devices and electrodes, J. Power Sources. 196 (2011) 1–12. https://doi.org/10.1016/j.jpowsour.2010.06.084.
[72] K.W. Nam, M.G. Kim, K.B. Kim, In situ Mn K-edge X-ray absorption spectroscopy studies of electrodeposited manganese oxide films for electrochemical capacitors, J. Phys. Chem. C. 111 (2007) 749–758. https://doi.org/10.1021/jp063130o.
[73] M. Toupin, T. Brousse, D. Bélanger, Charge storage mechanism of MnO_2 electrode used in aqueous electrochemical capacitor, Chem. Mater. 16 (2004) 3184–3190. https://doi.org/10.1021/cm049649j.
[74] S.-L. Kuo, N.-L. Wu, Investigation of Pseudocapacitive Charge-Storage Reaction of $MnO{\cdot}nH_2O$ Supercapacitors in Aqueous Electrolytes, J. Electrochem. Soc. 153 (2006) A1317. https://doi.org/10.1149/1.2197667.
[75] R.S. Kalubarme, H.S. Jadhav, C.J. Park, Electrochemical characteristics of two-dimensional nano-structured MnO2for symmetric supercapacitor, Electrochim. Acta. 87 (2013) 457–465. https://doi.org/10.1016/j.electacta.2012.09.081.
[76] S. Maiti, A. Pramanik, S. Mahanty, Influence of imidazolium-based ionic liquid electrolytes on the performance of nano-structured MnO_2 hollow spheres as electrochemical supercapacitor, RSC Adv. 5 (2015) 41617–41626. https://doi.org/10.1039/C5RA05514H.
[77] M.T. Lee, W.T. Tsai, M.J. Deng, H.F. Cheng, I.W. Sun, J.K. Chang, Pseudocapacitance of MnO_2 originates from reversible insertion/desertion of thiocyanate anions studied using in situ X-ray absorption spectroscopy in ionic liquid electrolyte, J. Power Sources. 195 (2010) 919–922. https://doi.org/10.1016/j.jpowsour.2009.08.047.
[78] C.A. Castro Ruiz, D. Bélanger, D. Rochefort, Electrochemical and spectroelectrochemical evidence of redox transitions involving protons in thin MnO_2 electrodes in protic ionic liquids, J. Phys. Chem. C. 117 (2013) 20397–20405. https://doi.org/10.1021/jp405047g.
[79] D. Majumdar, M. Mandal, S.K. Bhattacharya, V2O5 and its carbon-based nanocomposites for supercapacitor applications, ChemElectroChem. 6 (2019) 1623–1648. https://doi.org/10.1002/celc.201801761.
[80] M. Fehse, S. Cavaliere, P.E. Lippens, I. Savych, A. Iadecola, L. Monconduit, D.J. Jones, J. Rozière, F. Fischer, C. Tessier, L. Stievano, Nb-doped TiO_2 nanofibers for

lithium ion batteries, J. Phys. Chem. C. 117 (2013) 13827–13835. https://doi.org/10.1021/jp402498p.
[81] Z. Hu, X. Xiao, C. Chen, T. Li, L. Huang, C. Zhang, J. Su, L. Miao, J. Jiang, Y. Zhang, J. Zhou, Al-doped α-MnO_2 for high mass-loading pseudocapacitor with excellent cycling stability, Nano Energy. 11 (2015) 226–234. https://doi.org/10.1016/j.nanoen.2014.10.015.
[82] X. Chen, L. Liu, F. Huang, Black titanium dioxide (TiO_2) nanomaterials, Chem. Soc. Rev. 44 (2015) 1861–1885. https://doi.org/10.1039/c4cs00330f.
[83] J.G. Wang, Y. Yang, Z.H. Huang, F. Kang, A high-performance asymmetric supercapacitor based on carbon and carbon-MnO_2 nanofiber electrodes, Carbon N. Y. 61 (2013) 190–199. https://doi.org/10.1016/j.carbon.2013.04.084.
[84] Y. Cai, B. Zhao, J. Wang, Z. Shao, Non-aqueous hybrid supercapacitors fabricated with mesoporous TiO_2 microspheres and activated carbon electrodes with superior performance, J. Power Sources. 253 (2014) 80–89. https://doi.org/10.1016/j.jpowsour.2013.11.097.
[85] X. Wang, C. Yan, J. Yan, A. Sumboja, P.S. Lee, Orthorhombic niobium oxide nanowires for next generation hybrid supercapacitor device, Nano Energy. 11 (2015) 765–772. https://doi.org/10.1016/j.nanoen.2014.11.020.
[86] P. Han, G. Xu, X. Han, J. Zhao, X. Zhou, G. Cui, Lithium Ion Capacitors in Organic Electrolyte System: Scientific Problems, Material Development, and Key Technologies, Adv. Energy Mater. 8 (2018) 1–30. https://doi.org/10.1002/aenm.201801243.
[87] D. Ma, Z. Cao, A. Hu, Si-based anode materials for li-ion batteries: A mini review, Nano-Micro Lett. 6 (2014) 347–358. https://doi.org/10.1007/s40820-014-0008-2.
[88] A.J. Gardecka, M. Lübke, C.F. Armer, D. Ning, M. V. Reddy, A.S. Williams, A. Lowe, Z. Liu, I.P. Parkin, J.A. Darr, Nb-doped rutile titanium dioxide nanorods for lithium-ion batteries, Solid State Sci. 83 (2018) 115–121. https://doi.org/10.1016/j.solidstatesciences.2018.07.004.
[89] M. Wagemaker, R. Van de Krol, A.P.M. Kentgens, A.A. Van Well, F.M. Mulder, Two phase morphology limits lithium diffusion in TiO_2 (anatase): A 7Li MAS NMR study, J. Am. Chem. Soc. 123 (2001) 11454–11461. https://doi.org/10.1021/ja0161148.
[90] P. Simon, Y. Gogotsi, B. Dunn, Where Do Batteries End and Supercapacitors Begin ?, Science (80-.). 343 (2014) 1210–1211. https://doi.org/10.1126/science.1249625.
[91] M. Okubo, E. Hosono, J. Kim, M. Enomoto, N. Kojima, T. Kudo, H. Zhou, I. Honma, Nanosize effect on high-rate Li-ion intercalation in $LiCoO_2$ electrode, J. Am. Chem. Soc. 129 (2007) 7444–7452. https://doi.org/10.1021/ja0681927.
[92] H. Liu, F.C. Strobridge, O.J. Borkiewicz, K.M. Wiaderek, K.W. Chapman, P.J. Chupas, C.P. Grey, Capturing metastable structures during high-rate cycling of $LiFePO_4$ nanoparticle electrodes, Science (80-.). 344 (2014) 1252817–1252817. https://doi.org/10.1126/science.1252817.
[93] H. Kim, K.Y. Park, M.Y. Cho, M.H. Kim, J. Hong, S.K. Jung, K.C. Roh, K. Kang, High-performance hybrid supercapacitor based on graphene-wrapped $Li_4Ti_5O_{12}$ and activated carbon, ChemElectroChem. 1 (2014) 125–130. https://doi.org/10.1002/celc.201300186.
[94] V. Khomenko, E. Raymundo-Piñero, F. Béguin, High-energy density graphite/AC capacitor in organic electrolyte, J. Power Sources. 177 (2008) 643–651. https://doi.org/10.1016/j.jpowsour.2007.11.101.
[95] B.M. Jun, S. Kim, J. Heo, C.M. Park, N. Her, M. Jang, Y. Huang, J. Han, Y. Yoon, Review of MXenes as new nanomaterials for energy storage/delivery and selected environmental applications, Nano Res. 12 (2019) 471–487.

https://doi.org/10.1007/s12274-018-2225-3.
[96] Q. Jiang, N. Kurra, M. Alhabeb, Y. Gogotsi, H.N. Alshareef, All Pseudocapacitive MXene-RuO_2 Asymmetric Supercapacitors, Adv. Energy Mater. 8 (2018) 1–10. https://doi.org/10.1002/aenm.201703043.
[97] T. Nguyen, M. Boudard, M.J. Carmezim, M.F. Montemor, Layered $Ni(OH)_2$-$Co(OH)_2$ films prepared by electrodeposition as charge storage electrodes for hybrid supercapacitors, Sci. Rep. 7 (2017) 1–10. https://doi.org/10.1038/srep39980.
[98] M. Galiński, A. Lewandowski, I. Stepniak, Ionic liquids as electrolytes, Electrochim. Acta. 51 (2006) 5567–5580. https://doi.org/10.1016/j.electacta.2006.03.016.
[99] J. Krummacher, C. Schütter, S. Passerini, A. Balducci, Characterization of Different Conductive Salts in ACN-Based Electrolytes for Electrochemical Double-Layer Capacitors, ChemElectroChem. 4 (2017) 353–361. https://doi.org/10.1002/celc.201600534.
[100] B. Pal, S. Yang, S. Ramesh, V. Thangadurai, R. Jose, Electrolyte selection for supercapacitive devices: A critical review, Nanoscale Adv. 1 (2019) 3807–3835. https://doi.org/10.1039/c9na00374f.
[101] M. Endo, T. Maeda, T. Takeda, Y.J. Kim, K. Koshiba, H. Hara, M.S. Dresselhaus, Capacitance and Pore-Size Distribution in Aqueous and Nonaqueous Electrolytes Using Various Activated Carbon Electrodes, J. Electrochem. Soc. 148 (2001) A910. https://doi.org/10.1149/1.1382589.
[102] K.O. Oyedotun, T.M. Masikhwa, S. Lindberg, A. Matic, P. Johansson, N. Manyala, Comparison of ionic liquid electrolyte to aqueous electrolytes on carbon nanofibres supercapacitor electrode derived from oxygen-functionalized graphene, Chem. Eng. J. 375 (2019). https://doi.org/10.1016/j.cej.2019.121906.
[103] F.B. Sillars, S.I. Fletcher, M. Mirzaeian, P.J. Hall, Effect of activated carbon xerogel pore size on the capacitance performance of ionic liquid electrolytes, Energy Environ. Sci. 4 (2011) 695–706. https://doi.org/10.1039/c0ee00337a.
[104] E.Y. Tyunina, M.D. Chekunova, V.N. Afanasiev, Electrochemical characteristics of propylene carbonate solutions of tetraethylammonium tetrafluoroborate, Russ. J. Electrochem. 49 (2013) 453–457. https://doi.org/10.1134/S1023193513050157.
[105] D.I. Iermakova, R. Dugas, M.R. Palacín, A. Ponrouch, On the Comparative Stability of Li and Na Metal Anode Interfaces in Conventional Alkyl Carbonate Electrolytes, J. Electrochem. Soc. 162 (2015) A7060–A7066. https://doi.org/10.1149/2.0091513jes.
[106] W. Wu, S. Shabhag, J. Chang, A. Rutt, J.F. Whitacre, Relating Electrolyte Concentration to Performance and Stability for $NaTi_2(PO_4)_3$/$Na_{0.44}MnO_2$ Aqueous Sodium-Ion Batteries , J. Electrochem. Soc. 162 (2015) A803–A808. https://doi.org/10.1149/2.0121506jes.
[107] M. Brachet, T. Brousse, J. Le Bideau, All solid-state symmetrical activated carbon electrochemical double layer capacitors designed with ionogel electrolyte, ECS Electrochem. Lett. 3 (2014) A112–A115. https://doi.org/10.1149/2.0051411eel.
[108] M.J.M. Jafeen, M.A. Careem, S. Skaarup, Membrane hydration number of Li^+ ion in highly concentrated aqueous LiCl solutions, Ionics (Kiel). 25 (2019) 3453–3460. https://doi.org/10.1007/s11581-019-02876-y.
[109] J. Zheng, J.A. Lochala, A. Kwok, Z.D. Deng, J. Xiao, Research Progress towards Understanding the Unique Interfaces between Concentrated Electrolytes and Electrodes for Energy Storage Applications, Adv. Sci. 4 (2017) 1–19. https://doi.org/10.1002/advs.201700032.
[110] O.C. Okorafor, Solubility and density isotherms for the sodium sulfate-water-methanol system, J. Chem. Eng. Data. 44 (1999) 488–490. https://doi.org/10.1021/je980243v.
[111] L. Suo, O. Borodin, Y. Wang, X. Rong, W. Sun, X. Fan, S. Xu, M.A. Schroeder, A. V.

Cresce, F. Wang, C. Yang, Y.S. Hu, K. Xu, C. Wang, “Water-in-Salt” Electrolyte Makes Aqueous Sodium-Ion Battery Safe, Green, and Long-Lasting, Adv. Energy Mater. 7 (2017) 1–10. https://doi.org/10.1002/aenm.201701189.
[112] A. Gambou-Bosca, D. Bélanger, Electrochemical characterization of MnO_2-based composite in the presence of salt-in-water and water-in-salt electrolytes as electrode for electrochemical capacitors, J. Power Sources. 326 (2016) 595–603. https://doi.org/10.1016/j.jpowsour.2016.04.088.
[113] A. Yamada, K. Sodeyama, Y. Tateyama, J. Wang, Y. Yamada, C.H. Chiang, Superconcentrated electrolytes for a high-voltage lithium-ion battery, Nat. Commun. 7 (2016) 1–9. https://doi.org/10.1038/ncomms12032.
[114] J. Yin, C. Zheng, L. Qi, H. Wang, Concentrated NaClO4 aqueous solutions as promising electrolytes for electric double-layer capacitors, J. Power Sources. 196 (2011) 4080–4087. https://doi.org/10.1016/j.jpowsour.2010.12.064.
[115] G. Wang, L. Fu, N. Zhao, L. Yang, Y. Wu, H. Wu, An aqueous rechargeable lithium battery with good cycling performance, Angew. Chemie - Int. Ed. 46 (2007) 295–297. https://doi.org/10.1002/anie.200603699.
[116] Y. Yamada, K. Furukawa, K. Sodeyama, K. Kikuchi, M. Yaegashi, Y. Tateyama, A. Yamada, Unusual stability of acetonitrile-based superconcentrated electrolytes for fast-charging lithium-ion batteries, J. Am. Chem. Soc. 136 (2014) 5039–5046. https://doi.org/10.1021/ja412807w.
[117] Q. Dou, S. Lei, D.W. Wang, Q. Zhang, D. Xiao, H. Guo, A. Wang, H. Yang, Y. Li, S. Shi, X. Yan, Safe and high-rate supercapacitors based on an “acetonitrile/water in salt” hybrid electrolyte, Energy Environ. Sci. 11 (2018) 3212–3219. https://doi.org/10.1039/c8ee01040d.
[118] A. Matic, B. Scrosati, Ionic liquids for energy applications, MRS Bull. 38 (2013) 533–537. https://doi.org/10.1557/mrs.2013.154.
[119] P.M. Dean, J.M. Pringle, D.R. MacFarlane, Structural analysis of low melting organic salts: Perspectives on ionic liquids, Phys. Chem. Chem. Phys. 12 (2010) 9144–9153. https://doi.org/10.1039/c003519j.
[120] A. Brandt, S. Pohlmann, A. Varzi, A. Balducci, S. Passerini, Ionic liquids in supercapacitors, MRS Bull. 38 (2013) 554–559. https://doi.org/DOI: 10.1557/mrs.2013.151.
[121] J. Chapman Varela, K. Sankar, A. Hino, X. Lin, W.S. Chang, D. Coker, M. Grinstaff, Piperidinium ionic liquids as electrolyte solvents for sustained high temperature supercapacitor operation, Chem. Commun. 54 (2018) 5590–5593. https://doi.org/10.1039/c8cc01093e.
[122] T. Welton, Ionic liquids: a brief history, Biophys. Rev. 10 (2018) 691–706. https://doi.org/10.1007/s12551-018-0419-2.
[123] P. Bonhôte, A.P. Dias, N. Papageorgiou, K. Kalyanasundaram, M. Grätzel, Hydrophobic, Highly Conductive Ambient-Temperature Molten Salts, Inorg. Chem. 35 (1996) 1168–1178. https://doi.org/10.1021/ic951325x.
[124] T.L. Greaves, C.J. Drummond, Protic ionic liquids: Properties and applications, Chem. Rev. 108 (2008) 206–237. https://doi.org/10.1021/cr068040u.
[125] T. Stettner, F.C. Walter, A. Balducci, Imidazolium-Based Protic Ionic Liquids as Electrolytes for Lithium-Ion Batteries, Batter. Supercaps. 2 (2019) 55–59. https://doi.org/10.1002/batt.201800096.
[126] M.F. El-Kady, V. Strong, S. Dubin, R.B. Kaner, Laser Scribing of High-Performance and Flexible Graphene-Based Electrochemical Capacitors, Science (80-.). 335 (2012) 1326–1330. https://doi.org/10.1126/science.1216744.
[127] N. Handa, T. Sugimoto, M. Yamagata, M. Kikuta, M. Kono, M. Ishikawa, A neat ionic

liquid electrolyte based on FSI anion for electric double layer capacitor, J. Power Sources. 185 (2008) 1585–1588. https://doi.org/10.1016/j.jpowsour.2008.08.086.
[128] S. Zhang, S. Brahim, S. Maat, High-voltage operation of binder-free CNT supercapacitors using ionic liquid electrolytes, J. Mater. Res. 33 (2018) 1179–1188. https://doi.org/10.1557/jmr.2017.455.
[129] A. Jänes, J. Eskusson, T. Thomberg, T. Romann, E. Lust, Ionic liquid-1,2-dimethoxyethane mixture as electrolyte for high power density supercapacitors, J. Energy Chem. 25 (2016) 609–614. https://doi.org/10.1016/j.jechem.2016.02.011.
[130] C. Largeot, P.L. Taberna, Y. Gogotsi, P. Simon, Microporous carbon-based electrical double layer capacitor operating at high temperature in ionic liquid electrolyte, Electrochem. Solid-State Lett. 14 (2011) 174–177. https://doi.org/10.1149/2.013112esl.
[131] M. Haque, Q. Li, A.D. Smith, V. Kuzmenko, E. Köhler, P. Lundgren, P. Enoksson, Thermal influence on the electrochemical behavior of a supercapacitor containing an ionic liquid electrolyte, Electrochim. Acta. 263 (2018) 249–260. https://doi.org/10.1016/j.electacta.2018.01.029.
[132] G.A. dos Santos Junior, V.D.S. Fortunato, G.G. Silva, P.F.R. Ortega, R.L. Lavall, High-performance Li-Ion hybrid supercapacitor based on LiMn2O4 in ionic liquid electrolyte, Electrochim. Acta. 325 (2019) 134900. https://doi.org/10.1016/j.electacta.2019.134900.
[133] S. Menne, J. Pires, M. Anouti, A. Balducci, Protic ionic liquids as electrolytes for lithium-ion batteries, Electrochem. Commun. 31 (2013) 39–41. https://doi.org/10.1016/j.elecom.2013.02.026.
[134] R. Mysyk, E. Raymundo-Piñero, M. Anouti, D. Lemordant, F. Béguin, Pseudo-capacitance of nanoporous carbons in pyrrolidinium-based protic ionic liquids, Electrochem. Commun. 12 (2010) 414–417. https://doi.org/10.1016/j.elecom.2010.01.007.
[135] A. Brandt, J. Pires, M. Anouti, A. Balducci, An investigation about the cycling stability of supercapacitors containing protic ionic liquids as electrolyte components, Electrochim. Acta. 108 (2013) 226–231. https://doi.org/10.1016/j.electacta.2013.06.118.
[136] L. Mayrand-Provencher, D. Rochefort, Influence of the Conductivity and Viscosity of Protic Ionic Liquids Electrolytes on the Pseudocapacitance of RuO_2 Electrodes, J. Phys. Chem. C. 113 (2009) 1632–1639. https://doi.org/10.1021/jp8084149.
[137] B. Gélinas, D. Rochefort, Synthesis and characterization of an electroactive ionic liquid based on the ferrocenylsulfonyl(trifluoromethylsulfonyl)imide anion, Electrochim. Acta. 162 (2015) 36–44. https://doi.org/10.1016/j.electacta.2014.11.154.
[138] E. Mourad, L. Coustan, P. Lannelongue, D. Zigah, A. Mehdi, A. Vioux, S.A. Freunberger, F. Favier, O. Fontaine, Biredox ionic liquids with solid-like redox density in the liquid state for high-energy supercapacitors, Nat. Mater. 16 (2017) 446–454. https://doi.org/10.1038/NMAT4808.
[139] G. Inzelt, Pseudo-reference electrodes, in: G. Inzelt, A. Lewenstam, F. Scholz (Eds.), Handb. Ref. Electrodes, Springer Berlin Heidelberg, Berlin, Heidelberg, 2013: pp. 331–332. https://doi.org/10.1007/978-3-642-36188-3_14.
[140] M. Vijayakumar, R. Santhosh, J. Adduru, T.N. Rao, M. Karthik, Activated carbon fibres as high performance supercapacitor electrodes with commercial level mass loading, Carbon N. Y. 140 (2018) 465–476. https://doi.org/10.1016/j.carbon.2018.08.052.
[141] N. Elgrishi, K.J. Rountree, B.D. McCarthy, E.S. Rountree, T.T. Eisenhart, J.L. Dempsey, A Practical Beginner's Guide to Cyclic Voltammetry, J. Chem. Educ. 95 (2018) 197–206. https://doi.org/10.1021/acs.jchemed.7b00361.

[142] F. Scholz, Electroanalytical Methods - Guide to Experiments and Applications, 2nd ed., Springer, 2010. https://doi.org/10.1007/978-3-642-02915-8.
[143] T.S. Mathis, N. Kurra, X. Wang, D. Pinto, P. Simon, Y. Gogotsi, Energy Storage Data Reporting in Perspective—Guidelines for Interpreting the Performance of Electrochemical Energy Storage Systems, Adv. Energy Mater. 9 (2019) 1–13. https://doi.org/10.1002/aenm.201902007.
[144] K. Xu, M.S. Ding, T. Richard Jow, A better quantification of electrochemical stability limits for electrolytes in double layer capacitors, Electrochim. Acta. 46 (2001) 1823–1827. https://doi.org/10.1016/S0013-4686(01)00358-9.
[145] D. Weingarth, H. Noh, A. Foelske-Schmitz, A. Wokaun, R. Kötz, A reliable determination method of stability limits for electrochemical double layer capacitors, Electrochim. Acta. 103 (2013) 119–124. https://doi.org/10.1016/j.electacta.2013.04.057.
[146] P. Ratajczak, K. Jurewicz, P. Skowron, Q. Abbas, F. Béguin, Effect of accelerated ageing on the performance of high voltage carbon/carbon electrochemical capacitors in salt aqueous electrolyte, Electrochim. Acta. 130 (2014) 344–350. https://doi.org/10.1016/j.electacta.2014.02.140.
[147] M.D. Stoller, R.S. Ruoff, Best practice methods for determining an electrode material's performance for ultracapacitors, Energy Environ. Sci. 3 (2010) 1294. https://doi.org/10.1039/c0ee00074d.
[148] E. Barsoukov, J.R. Macdonald, Impedance Spectroscopy : Theory, Experiment, and Applications, John Wiley & Sons, Incorporated, Hoboken, UNITED STATES, 2005. http://ebookcentral.proquest.com/lib/chalmers/detail.action?docID=226625.
[149] M. Pfanzelt, P. Kubiak, S. Jacke, L. Dimesso, W. Jaegermann, M. Wohlfahrt-Mehrens, SEI formation on TiO_2 rutile, J. Electrochem. Soc. 159 (2012) 809–814. https://doi.org/10.1149/2.085206jes.
[150] M. Rana, V. Sai Avvaru, N. Boaretto, V.A. De La Peña O'Shea, R. Marcilla, V. Etacheri, J.J. Vilatela, High rate hybrid MnO_2@CNT fabric anodes for Li-ion batteries: Properties and a lithium storage mechanism study by: In situ synchrotron X-ray scattering, J. Mater. Chem. A. 7 (2019) 26596–26606. https://doi.org/10.1039/c9ta08800h.
[151] Y. Yuan, C. Zhan, K. He, H. Chen, W. Yao, S. Sharifi-Asl, B. Song, Z. Yang, A. Nie, X. Luo, H. Wang, S.M. Wood, K. Amine, M.S. Islam, J. Lu, R. Shahbazian-Yassar, The influence of large cations on the electrochemical properties of tunnel-structured metal oxides, Nat. Commun. 7 (2016) 1–9. https://doi.org/10.1038/ncomms13374.
[152] N. Zec, N. Cvjetićanin, M. Bešter-Rogač, M. Vraneš, S. Gadžurića, Electrochemical performance of anatase TiO_2 nanotube arrays electrode in ionic liquid based electrolyte for lithium ion batteries, J. Electrochem. Soc. 164 (2017) H5100–H5107. https://doi.org/10.1149/2.0051708jes.
[153] N.M. Ndiaye, T.M. Masikhwa, B.D. Ngom, M.J. Madito, K.O. Oyedotun, J.K. Dangbegnon, N. Manyala, Effect of growth time on solvothermal synthesis of vanadium dioxide for electrochemical supercapacitor application, Mater. Chem. Phys. 214 (2018) 192–200. https://doi.org/10.1016/j.matchemphys.2018.04.087.